WARWICK
THE UNIVERSITY OF WARWICK

Manuscript version: Author's Accepted Manuscript
The version presented in WRAP is the author's accepted manuscript and may differ from the published version or Version of Record.

Persistent WRAP URL:
http://wrap.warwick.ac.uk/116554

How to cite:
Please refer to published version for the most recent bibliographic citation information. If a published version is known of, the repository item page linked to above, will contain details on accessing it.

Copyright and reuse:
The Warwick Research Archive Portal (WRAP) makes this work by researchers of the University of Warwick available open access under the following conditions.

Copyright © and all moral rights to the version of the paper presented here belong to the individual author(s) and/or other copyright owners. To the extent reasonable and practicable the material made available in WRAP has been checked for eligibility before being made available.

Copies of full items can be used for personal research or study, educational, or not-for-profit purposes without prior permission or charge. Provided that the authors, title and full bibliographic details are credited, a hyperlink and/or URL is given for the original metadata page and the content is not changed in any way.

Publisher's statement:
Please refer to the repository item page, publisher's statement section, for further information.

For more information, please contact the WRAP Team at: wrap@warwick.ac.uk.

warwick.ac.uk/lib-publications

TOPICAL REVIEW

Molecular Simulation of Liquid Crystals

Michael P. Allen

Department of Physics, University of Warwick, Coventry CV4 7AL, U. K., *and*
H. H. Wills Physics Laboratory, Royal Fort, Tyndall Avenue, Bristol BS8 1TL, U. K.

ARTICLE HISTORY
Compiled April 20, 2019

ABSTRACT
This article reviews recent progress in the computer simulation of liquid crystals at the molecular level. It covers the use of simple rigid-body models of the constituent molecules, and more detailed modelling via atomistic force fields. Bulk mesophases, inhomogeneous systems, and interfaces, are discussed. Recent progress in calculating elastic properties and dynamics is summarized. As well as presenting an overview, some specific topics of recent interest are highlighted: the biaxial nematic phase, chiral phases, ionic liquid crystals, and charge-transfer systems.

KEYWORDS
Liquid crystals, molecular dynamics, Monte Carlo, molecular simulation

1. Introduction

Liquid crystals were recognized as mesophases, having properties intermediate between liquids and solids, in the late 19th century, and following a long period in which they remained of academic interest only, they began to grow rapidly in importance in the 1970s [1]. This was due to two factors: the synthesis of molecules that exhibited interesting mesophases at room temperature, and the development of possible technological applications based on twist cells. Although techniques for simulating molecular liquids [2, 3] were by then well established, it was not until the mid-1980s that the first off-lattice molecular simulations of liquid crystal phases were carried out. This was mainly due to the intrinsically long time scales and length scales associated with equilibration of mesophases and with many of their interesting properties, such as hydrodynamic flow, director reorientation, and defect structures. Much of the interesting physics behind the mesoscopic and macroscopic behaviour of liquid crystals is well understood [4] but the link between their thermodynamic stability and properties and the detailed structure of the constituent molecules, remains a challenge which molecular simulation is well placed to address. With the inexorable growth of computer power over the last 35 years, the field has developed strikingly, and several reviews have appeared [5–11]. This review will look at developments over the last decade, with some reference to earlier papers in order to provide historical context and background information. The term 'liquid crystals' includes thermotropic materials, and also colloidal suspensions of non-spherical micron-scale particles and viruses.

Email: m.p.allen@warwick.ac.uk and m.p.allen@bristol.ac.uk

To keep the review within reasonable bounds, it will concentrate on models using freely translating and rotating objects, which attempt to represent the shape and structure of a molecule, or colloidal particle. Unfortunately, there will be no room to discuss interesting recent work based on continuum descriptions [12], lattice spin models [13], or mesoscale methods such as lattice Boltzmann simulations [14] and multi-particle collision dynamics [15]. Simulations of amphiphilic molecules [16] are out of scope, although the growing interest in ionic and polar liquid crystals has led to the inclusion of some examples which are on the border with this field. Again, for reasons of space, the interesting topics of chromonic liquid crystals [17] and polymer liquid crystals [18] cannot be included. While confined liquid crystals are mentioned, simulations of purely two-dimensional systems have had to be omitted.

The review is organized as follows. Sections 2–4 introduce the most commonly-used molecular models in increasing order of complexity: simple rigid particles, rigid and semiflexible chains, and atomistic force fields. In each case, references will be made to the corresponding mesophases. Sections 5 and 6 highlight two areas in which significant recent progress has been made: investigating the features which stabilize the biaxial nematic phase, and simulating chiral phases, respectively. Section 7 covers simulations of liquid crystals at interfaces, and confined in different geometries, including the case of embedded nanoparticles. The use of simulations to investigate elastic and dynamical properties of mesophases is covered in section 8. Finally, sections 9 and 10 outline two topics which seem to have grown significantly in importance over the last few years: ionic liquid crystals and charge transport.

2. Idealized models

Idealized models are frequently used to test theoretical predictions of phase stability and structure, demonstrate technical advances such as new methods of measuring properties, or provide insight into the fundamental origins of interesting behaviour. Some of these aspects will be covered in later sections. The rest of this section just summarizes recent work demonstrating mesophase stability for some of the standard models. Typical system sizes are 10^3–10^4 molecules, although somewhat larger systems are needed occasionally.

Two elementary atomic building blocks provide a convenient starting point. The hard sphere (HS) model is defined by a pair interaction

$$v_{\mathrm{HS}}(r_{ij}) = \begin{cases} \infty & r_{ij} < \sigma \\ 0 & r_{ij} \geq \sigma \end{cases} \tag{1}$$

where $r_{ij} = |\mathbf{r}_i - \mathbf{r}_j|$ is the interatomic distance between atoms i and j, and σ defines the atomic diameter. The Lennard-Jones (LJ) potential is

$$v_{\mathrm{LJ}}(r_{ij}) = 4\epsilon \left[\left(\frac{\sigma}{r_{ij}} \right)^{12} - \left(\frac{\sigma}{r_{ij}} \right)^{6} \right] \tag{2}$$

where ϵ defines the attractive well depth. Usually this is implemented with a cutoff

distance r_c, and is shifted so as to be zero at that point:

$$v_{LJ}^{s}(r_{ij}) = \begin{cases} v_{LJ}(r_{ij}) - v_{LJ}(r_c) & r_{ij} < r_c \\ 0 & r_{ij} \geq r_c. \end{cases} \quad (3)$$

A special case of this is the purely repulsive WCA potential [19]

$$v_{WCA}(r_{ij}) = \begin{cases} v_{LJ}(r_{ij}) + \epsilon & r_{ij} < 2^{1/6}\sigma \\ 0 & r_{ij} \geq 2^{1/6}\sigma. \end{cases} \quad (4)$$

Molecular models may be built out of atomic units of this kind. For example, linear rigid rods of repulsive and/or attractive beads [20–22] form isotropic (I), nematic (N), and smectic (Sm) phases. A 5×5 square array of WCA spheres [23] shows evidence of both columnar (Col) and cubatic phases. Semiflexible chains of atoms with angle-bending potentials, derived from simple bead-spring models of polymers [24], may produce mesogenic shapes (see section 3). Ultimately, one may construct a detailed atomic force field (see section 4).

The alternative approach is to use a single, non-spherical, rigid unit to represent each molecule. The configuration is therefore specified by the centre-of-mass positions $\mathbf{r}_i$ of each molecule i and, for axially symmetric particles, a unit vector $\mathbf{u}_i$ along the molecular axis. For molecules without axial symmetry, the orientation may be specified as a 3×3 rotation matrix, a set of three Euler angles, or four quaternion parameters [2].

One simple possibility is to start with the Lennard-Jones interaction, and modify the attractive term, multiplying it by a rotationally-invariant function of the angles, typically of second rank [25]. Such a potential is computationally inexpensive, has been shown to generate mesophases, and may be useful when a 'generic' off-lattice liquid crystal is of interest [26] (see also section 7.2). However, the more usual starting point is to make the repulsive core of the molecule nonspherical, and the rest of this section will concentrate on models of this kind.

2.1. Simple molecular shapes

Simple hard particle models have played an essential role in understanding the physics of liquid crystals. Partly this stems from Onsager's seminal theory paper [27], a forerunner of modern density functional theories [28, 29], which showed that sufficiently long hard rods would undergo an I–N transition, driven by the balance between translational and rotational entropy. Following the earliest simulations of the hard sphere system [30, 31], the repulsive interactions determining molecular size and shape were established as the main factor determining structure in the liquid state, underpinning perturbation theories of the thermodynamics and phase behaviour [32]. The first attempts to simulate mesophases using hard ellipsoids and spherocylinders [33, 34] were hampered by limited available computer power. However, eventually the nematic discotic (N_D) phase was successfully simulated for thin hard disks [35, 36], as well as both N and N_D phases for hard uniaxial ellipsoids of various aspect ratios [37, 38]. This model has been revisited recently [39, 40]. No translationally-ordered fluid mesophases of hard ellipsoids have been observed to date. However, other hard particles of various shapes have been shown to produce a range of mesophases [41–43]. A topical review on this subject has recently appeared [44].

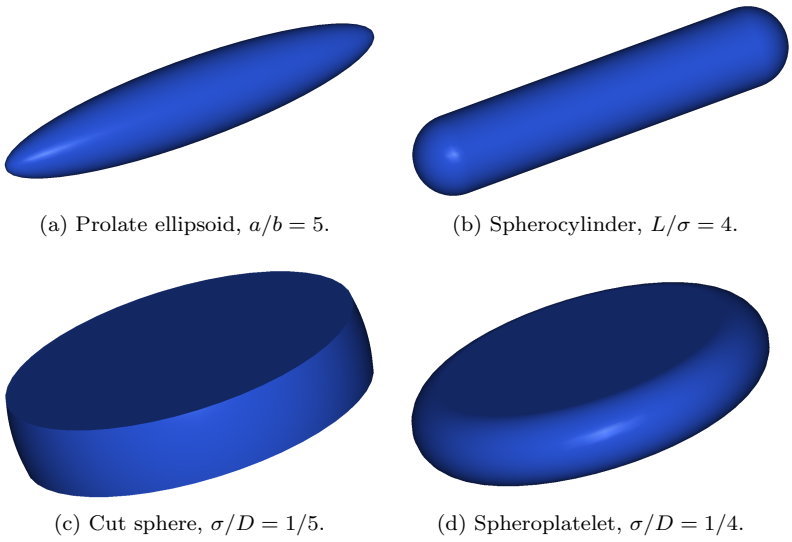

(a) Prolate ellipsoid, $a/b = 5$.

(b) Spherocylinder, $L/\sigma = 4$.

(c) Cut sphere, $\sigma/D = 1/5$.

(d) Spheroplatelet, $\sigma/D = 1/4$.

Figure 1. Example shapes used in hard-particle simulations. Figures produced using QMGA [50].

For hard particles, MC programs are quite simple, the key step being the criterion for overlap between a pair of particles. Some subtleties exist in the calculation of pressure in constant-volume simulations [45]. These models may also be studied by event-driven MD, which typically assumes free flight between instantaneous collisions [46–49]. Once more, in most cases, efficient detection of overlap between pairs is a key step.

For ellipsoids, suitable overlap prescriptions exist [33, 51], given the principal semi-axes a, b, c. For the uniaxial case, $b = c$, the shape is typically specified as an aspect ratio $\kappa = a/b$, which may be > 1 (prolate or calamitic, see Fig. 1(a)) or < 1 (oblate or discotic). An approximate ellipsoid overlap criterion, termed the hard Gaussian overlap (HGO) model, is based on the Berne–Pechukas [52] contact distance

$$\sigma_{\mathrm{BP}}(\hat{\mathbf{r}}_{ij}, \mathbf{u}_i, \mathbf{u}_j) = \sigma_0 \left[1 - \frac{1}{2}\chi \left\{ \frac{(\hat{\mathbf{r}}_{ij} \cdot \mathbf{u}_i + \hat{\mathbf{r}}_{ij} \cdot \mathbf{u}_j)^2}{1 + \chi\, \mathbf{u}_i \cdot \mathbf{u}_j} + \frac{(\hat{\mathbf{r}}_{ij} \cdot \mathbf{u}_i - \hat{\mathbf{r}}_{ij} \cdot \mathbf{u}_j)^2}{1 - \chi\, \mathbf{u}_i \cdot \mathbf{u}_j} \right\} \right]^{-1/2} \tag{5}$$

where $\hat{\mathbf{r}}_{ij} = \mathbf{r}_{ij}/r_{ij}$ is the unit vector corresponding to the separation $\mathbf{r}_{ij} = \mathbf{r}_i - \mathbf{r}_j$, and $\chi = (\kappa^2 - 1)/(\kappa^2 + 1)$. Overlap occurs when $r_{ij} < \sigma_{\mathrm{BP}}(\hat{\mathbf{r}}_{ij}, \mathbf{u}_i, \mathbf{u}_j)$. For any side-by-side arrangement, with $\hat{\mathbf{r}}_{ij} \cdot \mathbf{u}_i = \hat{\mathbf{r}}_{ij} \cdot \mathbf{u}_j = 0$, $\sigma_{\mathrm{BP}} = \sigma_0$. For the end-to-end arrangement (or face-to-face, for oblate particles), with $\hat{\mathbf{r}}_{ij} \cdot \mathbf{u}_i = \hat{\mathbf{r}}_{ij} \cdot \mathbf{u}_j = \mathbf{u}_i \cdot \mathbf{u}_j = 1$, $\sigma_{\mathrm{BP}} = \kappa\sigma_0$, as expected for ellipsoids of aspect ratio κ. However, for more general orientations, the agreement with hard ellipsoids is not exact. This model, and an improvement designed as a better fit to true ellipsoids, have been studied recently [53–55].

For spherocylinders, shown in Fig. 1(b), the unit vector $\mathbf{u}_i$ specifies the direction of a line segment of length L, and overlap is defined to occur when the shortest distance s_{ij} between two line segments satisfies $s_{ij} < \sigma$. The shape is therefore specified by the ratio L/σ, and the overall length-to-width ratio is $(L + \sigma)/\sigma$. Hard spherocylinders were shown to have N and smectic-A (SmA) phases [56–58]. Some early simulations suggesting the possibility of a columnar phase for spherocylinders seem to have suffered from finite-size effects, and similar considerations apply to other prolate hard shapes [59].

The cut sphere, a discotic model, shown in Fig. 1(c), is defined as the equatorial section of thickness σ delimited by two symmetrical parallel planar cuts through a

sphere of diameter D; the thickness-to-width ratio is therefore σ/D. Early simulations of hard cut spheres [60, 61] established N_D and columnar hexagonal (Col_h) phases for $\sigma/D = 0.1, 0.2$. In addition [61] for $\sigma/D = 0.2$, evidence was presented that the particles formed short stacks which could then arrange in a *cubatic* phase. For $0.1 \leq \sigma/D \leq 0.001$, umbrella sampling has been used [62, 63] to determine the free energy as a function of order parameter at the I–N_D transition. A minimum in the coexistence densities is seen as a function of aspect ratio, explained in terms of competition between the formation of large N_D regions, and short columnar stacks, in the isotropic phase. The issue of the cubatic phase has been re-examined [64]. Long simulations seem to establish a range of thicknesses for which the cubatic phase exists, stable relative to N_D. However, stability with respect to the competing Col phase has not been confimed, even using expanded ensemble techniques [65], and further simulations [66] suggest that it is only metastable. The N_D phase has been revisited [67] for thin platelets, as part of a broader study of percolation and orientational ordering [68, 69].

Spheroplatelets (sometimes called oblate spherocylinders) are shown in Fig. 1(d) and defined as follows. Given two thin circular disks of diameter D, it is possible to calculate the shortest distance s_{ij} between them: overlap occurs if $s_{ij} < \sigma$, where σ represents the thickness. The shape may be specified by σ/D, and the overall thickness-to-width ratio is $\sigma/(D + \sigma)$. Spheroplatelets with a range of aspect ratios have been studied [70, 71]. Col_h and N phases are observed for the thinner disks. Extensions of this model, incorporating continuous potentials of the Kihara type [72–74], exhibit the same mesophases. Binary mixtures of thin spheroplatelets and small hard spheres have also been studied [75] with a focus on I–N coexistence and stability against demixing.

Simple continuous interaction potentials may be devised by adapting hard-particle models. Often called Kihara potentials [76], they are typically written as LJ functions of s_{ij}/σ where σ is the thickness parameter and s_{ij} the shortest distance between the particle cores (line segments of length L in the case of spherocylinders, and thin discs of diameter D for spheroplatelets). Continuous, but almost athermal, analogues of the hard particles are obtained by choosing the WCA formula, eqn (4). These will be referred to as the WCA-SC and WCA-SP models. The phase diagram for WCA-SC has been compared with hard spherocylinders [77], and is rather similar: N and SmA phases are seen. There has also been some interest in perfectly aligned WCA-SC particles, which seem to exhibit a SmB phase [78–81]. In a similar way, one may define a WCA-BP potential by inserting eqn (5) into eqn (4). A different adaption of hard spherocylinders, the square well line model [82], also shows N and Sm phases [83].

More complex particle shapes have been studied, and a broader range of mesophases observed. A modification of the HGO model, generating a pear-shaped molecule, has been shown to give N and interdigitated SmA_d phases [84]. For bowl-like shapes, there is competition between the N_D phase, and aggregation into clusters or even columns or wormlike chains of stacked bowls [85–89]. Disc-like particles defined by the intersection of two spheres [90] and thin disks with a hard sphere at the centre [91] both show N phases. Hard spherocylinders with a hard sphere at the centre, constrained to parallel alignment, show N, SmA, and (tilted) SmC phases [92]. For the freely-rotating version of this model, the tilted phase is also seen [59]; this work also indicates that the columnar phase originally reported is not stable, for either parallel or freely-rotating versions. Various amphiphilic molecular shapes have been modelled using hard spherical and nonspherical building blocks [93]. Bent-core systems have been modelled using a combination of spherocylinders and spheres [94].

2.2. Gay–Berne models

Turning to continuous-potential models of mesogens, the Gay–Berne (GB) model [95] has become the *de facto* standard. It resembles the LJ potential, eqn (2), but is generalized in two ways. Firstly, the (σ/r_{ij}) factor is replaced by the shifted form

$$\frac{\sigma_1}{r_{ij} - \sigma_{\mathrm{BP}}(\hat{\mathbf{r}}_{ij}, \mathbf{u}_i, \mathbf{u}_j) + \sigma_1} \tag{6}$$

where σ_{BP} is given by eqn (5). For prolate molecules, $\kappa > 1$, the universal choice in eqn (6) is $\sigma_1 = \sigma_0$, the side-by-side distance parameter appearing in eqn (5). For oblate molecules, $\kappa < 1$, the same choice was made in early GB simulations; however, a physically more reasonable choice [96] is to take $\sigma_1 = \kappa\sigma_0$, which represents the face-to-face characteristic distance, and this will be assumed in what follows, unless explicitly stated otherwise. Secondly, the energy parameter ϵ is also made orientation dependent. This last dependence is characterized by a parameter κ', which determines the ratio of well depths ϵ(side-by-side)/ϵ(end-to-end), and by two exponents conventionally denoted μ and ν. So in fact there is a family of GB potentials, identified by the notation GB$(\kappa, \kappa', \mu, \nu)$ [97]. This notation will be followed here. However, the suggestion of Ref. [97] to conventionally define κ' differently for oblate particles, making it always greater than 1, seems not to have been generally adopted. Since well depths, in the oblate case, typically satisfy ϵ(edge-to-edge) $<$ ϵ(face-to-face), it follows that $\kappa' < 1$, as well as $\kappa < 1$, in such cases.

Usually a spherical cutoff is applied at $r_{ij} = r_{\mathrm{c}}$ and the potential is shifted to be zero at that distance. The magnitude of the shift term is therefore orientation dependent. Early simulations used a quite small value, $r_{\mathrm{c}} = 4\sigma_0$ for $\kappa = 3$ [98–100], which corresponds to a discontinuity in the potential equal to 6% of the well depth, in the end-to-end arrangement. This makes a significant difference to the properties of the system, and a larger value of r_{c} is generally preferable. Deriving forces and torques from the potential is straightforward, if tedious [101] (see also [102] and [2, appendix C]). The GB potential is easily generalized to approximate a biaxial ellipsoid [103–105]. A core-softened version of the potential has been investigated [106], and other modifications have been suggested [107]. Uniaxial and biaxial models, based on the ellipsoid contact potential rather than the approximate eqn (5), have been proposed [108, 109]. A different potential, resembling GB but based on results from colloid science, has been devised [110, 111]. This RE-squared potential reduces, correctly, to the interaction between spherical particles at large separation, while being more closely related to the microscopic physics of interacting ellipsoids at short distance.

The original suggestion [95], GB(3,5,2,1), has a well-studied phase diagram [112], showing N and SmB (or solid) phases; other popular choices are GB(3,5,1,3) [98] which exhibits a wider nematic range and a SmA phase, and GB(4.4,20,1,1) [97] which shows N, SmA, and SmB phases; GB(3,5,1,2) has also been studied [101]. These models are used as testbeds for investigating many liquid crystal properties, and will appear in several later sections; reviews of related simulation work have appeared [5–10]. A recent study of GB(4.4,20,1,1) near the I–N–SmA triple point, used a novel method to determine the free energy in the SmA phase [113]. For oblate ($\kappa < 1$) models, $\mathrm{N_D}$ and $\mathrm{Col_h}$ phases are observed for GB(0.345,0.2,1,2) [96, 114] and for GB(0.345,0.2,1,3) [115]. Yet another version, GB(0.345,0.2,2,1), exhibits $\mathrm{N_D}$ and two *tilted* $\mathrm{Col_h}$ phases, one of which includes a helical component in the columnar structure [116]. Two of these parametrizations with the less realistic choice $\sigma_1 = \sigma_0$ have been studied:

GB(0.345,0.2,1,3) again shows N_D and Col phases [117, 118], while GB(0.345,0.2,1,2) shows N_D and rectangular columnar (Col_r) phases [119].

Bowl-shaped molecules have been simulated using an extended GB-type model [120]. Columns of polar stacked particles are observed; also three dimensional polar clusters of parallel columns can be seen.

2.3. Dipolar and quadrupolar rigid models

As part of the effort to understand the importance of the charge distribution in stabilizing mesophases and influencing their properties, there have been several studies of rigid bodies decorated with electrostatic multipoles. Early explorations of the phase diagrams of molecules with central axial dipoles, using hard spherocylinders [121] and the GB(3,5,2,1) model [122, 123] show that the Sm phases are stabilized relative to N, which may disappear completely. Molecular diffusion and rotation in dipolar GB(3,5,1,2) has been studied [124]. For central transverse dipoles [125, 126] the Sm phase is also stabilized, and chains of dipoles are seen within the layers. A terminal axial dipole in spherocylinders [127] stabilizes N relative to SmA and for GB(3,5,1,3) gives rise to the interdigitated SmA_d phase [128] characteristic of mesogens such as 4-n-octyl-4-cyanobiphenyl, 8CB (see later). More recently, GB(κ,5,2,1), $3 \leq \kappa \leq 4$, with an axial terminal dipole has been shown to exhibit various, different, interdigitated Sm phases [129].

An interesting topic has been the role of dipoles in stabilizing a tilted SmC phase. A single dipole seems ineffective, although a recent study claims a ferroelectric tilted Sm phase for GB(κ,5,2,1), $\kappa = 1.5, 2$, carrying a central axial dipole [130]. GB(3,5,1,3) with a well-separated pair of dipoles, either axial or tilted relative to the axis, has been shown to produce tilted Sm phases [130, 131]. Simulations of GB(κ,5,2,1), $\kappa = 3, 4, 5$, with a pair of terminal antiparallel dipoles [132] also seem to generate tilted Sm phases. This has stimulated some discussion of the possible role of the freezing of rotational motion about the axis, in stabilizing such phases [133, 134]. (Tilted phases have also been observed for GB(4,5,2,1) with a central longitudinal *quadrupole* [135].) Also an interesting polarizable model based on parallel hard spherocylinders carrying opposite charges close to the ends [136] has been shown to exhibit a variety of phases including a SmC.

The search for a ferroelectric N phase, in which the molecular dipoles spontaneously align, has so far been unsuccessful. For the discotic model GB(0.345,0.2,1,3) with two parallel dipoles, placed symmetrically on the equatorial plane, slab-like domains of opposite polarization are formed [137–139]. The growth of these domains with system size is suggestive of long-range ferroelectric order.

The GB model has been used to aid interpretation of experimental NMR studies of solute orientational ordering and rotation in the N phase [140, 141]. A distribution of electrostatic quadrupoles is found to be a significant improvement over a single quadrupole in reproducing the sign of the experimentally observed orientational asymmetry coefficient.

3. Rigid and semiflexible chain models

Molecular flexibility is frequently cited as a factor stabilizing mesophases, relative to the solid, and a flexible alkyl tail is, of course, a feature of families of mesogens such as the alkyl-cyanobiphenyls, *n*CB. A simple way of studying this effect is to simulate

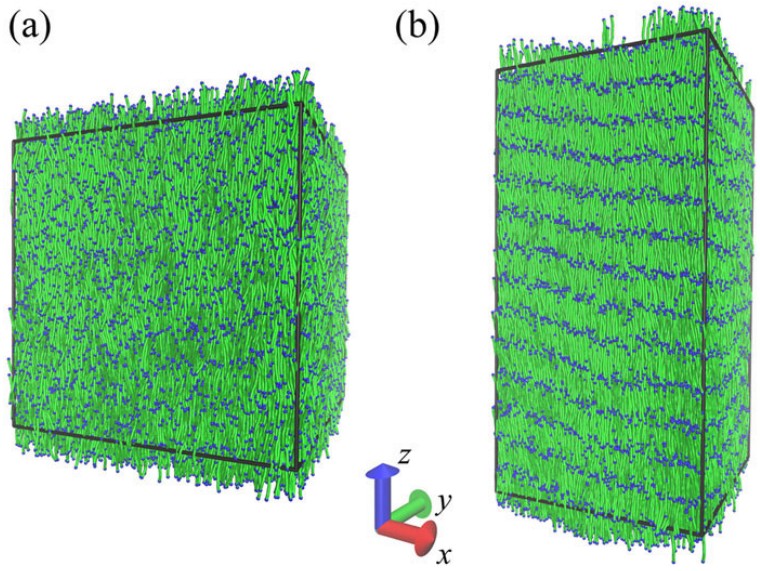

Figure 2. Snapshots of stiff FENE/WCA chains, each of 64 beads, in the (a) N and (b) Sm phases. Chain ends are colored blue to highlight Sm ordering in panel (b). A constant-pressure ensemble, with independently varying box lengths, is employed. Reprinted from Fig. 1 of A. Milchev, S.A. Egorov, K. Binder, and A. Nikoubashman, *J. Chem. Phys.,* **149,** 174909 (2018) [155] with the permission of AIP Publishing; permission conveyed through Copyright Clearance Center, Inc.

a chain of atoms, connected by fixed bond lengths, harmonic springs, or the FENE potential familiar from studies of flexible polymers [24]. Bond bending potentials may be used to adjust the flexibility. Comparison may then be made with completely rigid arrangements of spheres.

Early work on rods composed of fused hard spheres [142] indicated a N phase for sufficient rod length, while N and SmA phases were established for linear molecules composed of n tangent hard spheres for $n > 5$ [143–145]. Significantly extended studies of this model [146] showed amongst other things a maximum in the packing fraction change at the I–N transition for $n = 15$. The N phase was also established years ago for semiflexible chains, and chains composed of both rigid and flexible segments, with suitable parameters [144, 147–149]. Once more, a recent extended study [146] reveals in addition SmA and SmC phases. The I–N phase transition in binary mixtures of rigid and partially flexible hard-sphere chains has also been examined in detail [150].

Broadly similar behaviour is expected for chains composed of repulsive WCA beads. For example, in a system of nine overlapping beads, N, SmA, and crystal or SmB phases are seen [151, 152], the SmA being squeezed out when the flexibility increases. A recent larger-scale study of similar systems at various chain lengths [153] confirms this conclusion. Amongst various interesting trends discovered, under certain conditions the SmA layer spacing is found to increase with increasing density.

Extensive simulation studies of FENE/WCA chains have recently been reviewed [154]. This programme of work is notable for examining much larger systems than usual, extending the ranges of contour lengths and persistence lengths that are accessible. Specimen system sizes are 5000 chains, each consisting of 32–128 beads, and in some cases $\sim 1.6 \times 10^6$ monomers were employed; representative snapshots appear in Fig. 2. The bulk I–N transition has been studied in detail for a wide range of chain lengths and stiffness parameters [156]. Collective deflection fluctuations play an important role. The density of hairpin defects was found to decrease rapidly on moving deeper

into the N phase [155]; the chain persistence length was also found to be renormalized by orientational ordering. A Sm phase was also detected. This system has also been studied under confinement (see sections 7.2 and 7.3) and its elastic properties investigated (section 8.1).

Turning now to the effects of attractive interactions, the I–N transition for semi-flexible chains composed of hard spheres with square wells [157] and LJ atoms [158], have been studied. Rigid linear, and partially flexible, LJ chains also exhibit N–I coexistence [159] and some evidence of a SmC phase was found; binary mixtures of chains of different lengths were also studied.

4. Atomistic and coarse-grained models

Early, short (sub-nanosecond) atomistic simulations [160] concluded that observation of the *spontaneous* formation of a mesophase was beyond reach of accessible resources at the time. It took another seven years before this was achieved [161], and as a rough guideline, simulations of order 50 ns are now thought necessary to check mesophase stability [7]. With the steady increase of computer power, therefore, realistic atomic-level modelling of specific liquid crystalline systems has come within reach. The problem is still challenging: typically the goal is to reproduce the experimentally observed sequence of thermodynamically stable phases, and accurate phase transition temperatures (at least, at ambient pressure) not just for one system but for a family of molecules such as *n*CB. On top of this is the need to model translational and rotational dynamics as accurately as possible, and to make contact with experimental data such as the orientational distribution of dissolved dye molecules or spin probes. This desire for accuracy and transferability means that the standard force-fields built into simulation packages may not be sufficient: they are not optimized for liquid crystal properties, and some refinement is usually needed [7, 10]. A developing trend is the direct combination of simulations and experiments, as will become clear in some of the following examples.

Cacelli, Tani *et al.* have described an approach which emphasizes *ab initio* quantum chemistry [162]. Density functional calculations are used to optimize the geometry of a single molecule, calculate vibrational frequencies, the Hessian matrix, and carry out numerical fits to torsional energies. A fitting procedure is then used to deduce bond stretching, bending, and rigid-torsion force constants, as well as the form of flexible dihedral potentials. For inter-molecular potentials, an approach based on subdividing the molecule into fragments is adopted and a database of fragment–fragment interactions calculated for a wide range of configurations. These can either be generated for independent fragments, or for fragments already assembled into the constituent molecules. Such potentials have been used to model *n*CB ($n = 5, 6, 7, 8$) comparing with experimentally measured thermodynamics and structural properties [163–165], and transport coefficients [166]. The same force field was used to investigate the partial bilayer phase SmA_d of 8CB, consisting of pairs of interdigitated polar sublayers [167]. The approach has been extended to 5OCB [168], and an azoxybenzene derivative [169]. Although experimental transition temperatures could be reproduced within ± 10 K, and orientational order parameters were also in agreement with experiment, the liquid density was significantly overestimated, and this had a knock-on consequence for the dynamics.

More commonly, simulations are based on standard force-fields, with some parameters, for example the charge distribution, being refined according to quantum chem-

istry calculations. The AMBER force-field [170] which uses harmonic potentials for bond stretching and bending, and LJ potentials for non-bonded interactions, is a common choice. In the approach of Wilson *et al.* [171], density functional theory (DFT) calculations may be used to fit intramolecular force field parameters; in this case charges and van der Waals parameters were largely taken from the OPLS parameter set [172]. This force field has been used more recently [173] to simulate several fluoro-terphenyl derivatives. Similar phase sequences to experiment, N, SmA, and SmC, are seen, although the transition temperatures are not precisely reproduced. The degree of fluorine substitution is found to influence Sm layer formation, in agreement with experiment. Following the use of a similar force field to simulate the commercial liquid crystal mixture E7 [174], anthraquinone dye molecules in E7 [175–177] have been investigated recently. A separate calculation by dynamical DFT gave the orientation of the transition dipole vector within the dye, enabling comparison of order parameters with UV/visible spectroscopy. Trends, if not absolute values, agreed well with experiment, and a better understanding of the physical origin of molecular alignment came out of this combination of simulation and experiment. Continuing work of this kind has used an improved force field (see below). Dye molecule orientation in 5CB has also been simulated using GROMACS/OPLS-AA [178].

A notable success [179] was the prediction of the odd–even effect in transition temperatures for the phenyl-alkyl-4-(4'-cyanobenzylidene)aminocinnamate series. This work was based on AMBER/OPLS with geometrical parameters and partial charges determined quantum-mechanically.

A united-atom model of *n*CB molecules ($n = 4$–8) has been proposed by Tiberio *et al.* [180]. In the process of developing this, it was noted that the standard LJ parameters in the AMBER force field needed adjusting to improve the I–N transition temperature, electrostatic effects being of secondary importance here. Phase transition temperatures, orientational order parameter averages and distributions, structural correlation functions, dipolar coupling constants, and molecular dimensions, were all studied and compared, where possible, with experiment. 8CB has been studied over relatively long times, up to 400 ns [181]. N and $\mathrm{SmA_d}$ phases are seen, with transition temperatures in good agreement with experiment, and the interdigitation occurring in the latter phase was investigated in detail. Some comparison of both structure and dynamics with experimental measurements was possible. Since a united-atom model was employed, the timescales for dynamics are about an order of magnitude faster than in the real system, but trends with temperature are very similar.

This same model of 5CB [180] has been used to study a range of small rigid solute molecules, modelled in atomistic detail, in an attempt to rationalize the alignment mechanism [182]. In particular, comparison was made between simulations with and without an electrostatic charge distribution on the solute. Some comparison with experiment was possible, in terms of order parameters and dipolar couplings. Several theories of the effect were tested. A Maier–Saupe mean-field model seemed to be capable of reproducing the effective potential acting on the solutes, while the influence of electrostatics was found to be minimal. This suggests that the alignment is dominated by repulsive and van der Waals forces. A similar study was carried out of a flexible dopant, *n*-pentane [183]. Reasonable agreement of NMR dipolar coupling constants with experiment was obtained, although the molecular model proved slightly too rigid. Biphenyl solute molecules in 5CB and 8CB have been studied using the same approach [184]. Generally good agreement between simulation and experiment is achieved, when small corrections for solute-induced shifts in transition temperatures are made.

Experimental EPR spectra obtained from spin probe molecules have been usefully

compared with simulations of 5CB using GROMACS/OPLS-AA[185] and of 8CB using the General AMBER force field (GAFF) [186]. Particular attention was paid to the equilibration of N and SmA phases in the latter case, as well as assessing the importance of electrostatics (see also [187]). This combined EPR/MD approach has recently been reviewed [188].

The TraPPE-UA united-atom force field has been used to model 5CB and 8CB [189]. Comparisons with experiment are made of density, order parameter, N–I transition temperature, structure (through X-ray diffraction) and diffusion coefficients, for 5CB. Transferability to 8CB was demonstrated, showing the expected partially-interdigitated SmA_d phase.

An interesting development has been the adaptation of a polarizable force field originally developed for ionic liquids [190] so as to examine the influence of electrostatic interactions and polarizability on the behaviour of 5CB [191]. Phase transition temperatures, pairwise positional and orientational correlations, conformational properties, and diffusion coefficients, were compared with experiment. It was concluded that polarizability was *not* essential, but that a combination of reducing the dipole moments and dihedral potential barriers (compared with values initially suggested by quantum chemistry calculations) gave the best fit.

Turning away from the *n*CB family, high-temperature phases of sexithiophene have been simulated using the standard AMBER force field, with partial charges from quantum chemistry, and particular attention paid to the torsional potential between the thiophene rings [192]. N and SmA phases were observed and characterized; the molecule was found to adopt a bent shape in the liquid crystal. Overall, good agreement with experiment was found. A similar approach to quinquephenyl required more empirical adjustment of the force field [193]; N and two different Sm phases are observed. Although this molecule is frequently pictured as a rigid rod, the simulations suggest that flexibility, especially torsional motions around the axis, have a significant effect in stabilizing the N phase. A few other systems have been investigated using essentially standard force fields, based closely on the OPLS and OPLS-AA parameters. These include HO–6OCB and HO–7OCB [194] where hydrogen bonding enhances the local structure, and various ester derivatives [195–197] where the details of molecular structure may affect the tilt in the SmC phase.

Recently a further effort has been made to develop an accurate and transferable potential [198]. Based on GAFF, this addressed several factors which contribute to the overestimation of the I–N transition temperature: over-stiff alkyl chains, inflexible ester groups, over-attractive LJ parameters. The resulting force field, termed GAFF-LCFF, has been tested on a typical calamitic mesogen, 1,3-benzenedicarboxylic acid-1,3-bis(4-butylphenyl)-ester, containing aromatic and ester groups as well as flexible chains, and in simulations of dopants in E7 [177]. The force field has been further improved and applied to bent-core molecules [199]. Figure 3 illustrates the degree of agreement with the experimental transition temperature for a typical case, as well as the equilibration timescales in the vicinity of the transition.

Considerable progress has been made in recent years in the development of coarse-grained (CG) potentials, intended to speed up the simulations by discarding expensive details while retaining the essential physics of molecular interactions [200, 201]. An instructive example here is the azobenzene derivative, 8AB8 [202, 203]. These papers discuss some of the essential technicalities: the choice of reference state, and the trade-off between 'structural' and 'thermodynamic' targets for the coarse-graining, bearing in mind the aim of modelling a photo-induced phase transition. The dynamics of this model are discussed in section 8.2.

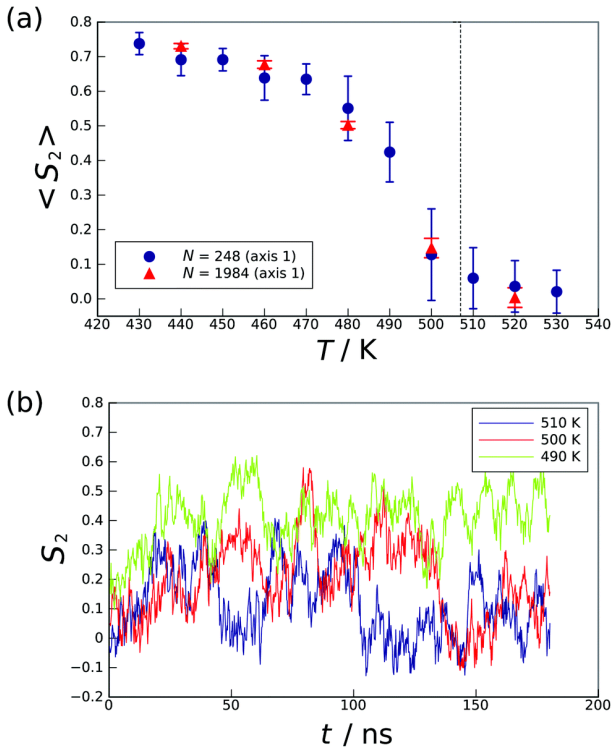

Figure 3. (a) Average uniaxial order parameters as a function of temperature for a bent-core bis-(phenyl)-oxadiazole derivative at two system sizes. The dotted line represents the experimental N–I transition temperature. (b) Order parameter as a function of time at temperatures close to the phase transition (248-molecule system). Republished by permission of the Royal Society of Chemistry from Fig. 8 of N.J. Boyd and M.R. Wilson, *Phys. Chem. Chem. Phys.*, **20,** 1485 (2018) [199]; permission conveyed through Copyright Clearance Center, Inc.

Reproducing the observed phase behaviour and transition temperatures of 5CB with a CG model has proved challenging [204]. An attempt has been made to combine both structure-based and thermodynamics-based coarse graining for 5CB [205], with some measure of transferability to 6CB and 8CB [206]. Another CG model of 5CB has been developed to help predict optical and dielectric properties [207]. A further example of CG modelling will appear in section 9.

The above methods employ atomistic simulations of the condensed phase as a reference, rather than developing an effective potential from averaged pair configurations (sometimes using umbrella sampling). An early example of the latter approach used Boltzmann-weighted sampling to fit the parameters of the GB potential to an atomistic model of *p*-terphenyl [208]. Similar approaches have appeared more recently for an oligomer of highly elongated units [209] and for a large disk-shaped molecule, coronene [210]. A semi-coarse-grained model has been used for molecules composed of 4-butyloxyphenyl and octyloxypyrimidine units [211]. The flexible chains are represented atomistically, while the phenyl and pyrimidine rings are modelled using GB units carrying multipole moments. The GB parameters are estimated from *ab initio* calculations of dimer configurations, and refined using bulk liquid simulations of benzene and biphenyl. The effects of the different ring configurations, as well as the presence of multipoles, on the observed N, SmA, and SmC phases, are discussed.

5. The biaxial nematic phase

The existence, or otherwise, of the biaxial nematic (N_b) phase has been a long-standing topic of interest; for a review of simulation activity see Ref. [212]. For hard particles, characterized by dimensions $a > b > c$, simple theories predict that it should be observed for the so-called 'dual' shape $b \sim \sqrt{ac}$. Early simulations of biaxial ellipsoids [213, 214] seemed to confirm this phase, in between N (for $b < \sqrt{ac}$) and N_D (for $b > \sqrt{ac}$) phases. By modern standards, these simulations were small and short in length; also, for this model, other competing phases such as SmA and Col_h are absent. Recently, attention has been given to the simulation of polyhedral, prism-, board- or plate-like shapes, which have a richer phase behaviour. Rod-like triangular prisms have both N and Sm phases [215]. Hard cuboidal board-like particles [216] exhibit a rich phase diagram, including N, N_D, rectangular columnar (Col_r) phases, and an interesting discotic Sm phase, in which the long axes of the particles are randomly oriented within the smectic layers. However, the Col phase reported for prolate particles now seems to have been a finite-size artefact [59]. Although some evidence was also obtained in favour of a biaxial smectic (SmA_b) phase, no N_b phase was seen for this model. Extending this study to binary mixtures of long and short particles [217] surprisingly showed Sm phases preferred over any nematics. Similarly-shaped particles, but with rounded corners [218, 219], show N, N_D, and SmA phases. In addition, near the 'dual' shape, a transition between two different N_b phases is claimed. Hard rhombic platelets of various thicknesses [220] show stable N_D, Sm and Col phases, together with evidence of a N_b phase for extremely thin platelets. Recently, convincing evidence has been presented of the N_b phase [221] for a range of polyhedra: cuboids, triangular prisms, and rhombic platelets. In all cases, the phase is stable near the so-called dual shape, and only appears if the particles are sufficiently anisotropic in shape; such systems are also highly responsive to weak aligning fields [222].

Ref. [212] reviews early efforts to simulate the N_b phase using the biaxial GB model. A recent study across a wide range of parameters has shed new light regarding the

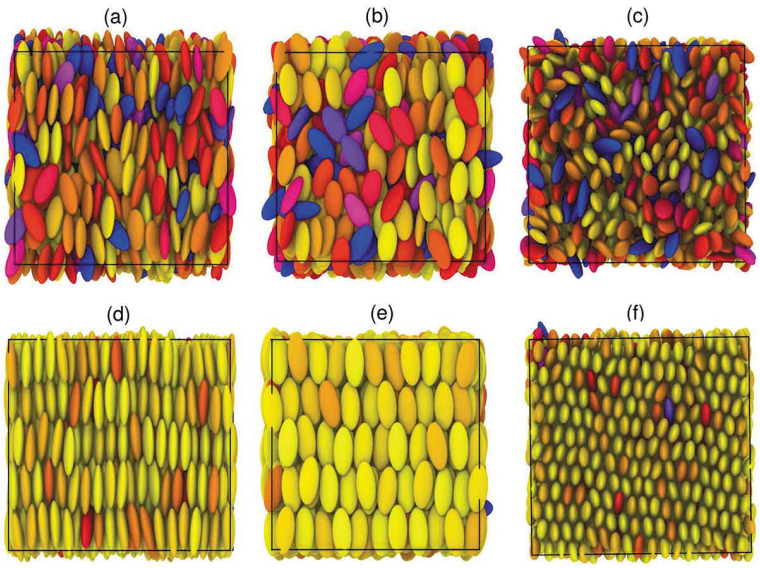

Figure 4. Snapshots of biaxial Gay–Berne particles, of relative axis lengths 1.4 : 0.714 : 3 and interaction energies 1 : 1.961 : 0.467. Phases are (a)–(c) a biaxial nematic N_b phase, and (d)–(f) a biaxial solid-like phase. In each case three orthogonal views are shown, each along a director. Particles are coloured according to the orientation of the longest axis with respect to the corresponding director. Reprinted from Fig. 5 of S. Orlandi, L. Muccioli, and R. Berardi, *Liq. Cryst.,* **45,** 2400 (2018) [223] with the permission of Taylor and Francis Ltd.; permission conveyed through Copyright Clearance Center, Inc.

combined effects of shape and the anisotropic nature of the attractions in determining the stability of N_b, along with other features of the complex phase diagram [223]. Representative snapshots appear in Fig. 4. Extending the parameter range clarified that it was *not* essential that shape and interaction biaxialities have opposite signs in order to stabilize N_b relative to competing translationally ordered phases, an impression that had arisen from earlier work on a smaller number of cases. It was also noted that, on cooling from the I phase, the N_b phase was never formed directly: a uniaxial ordered phase always intervened.

Central [224] and off-centre [225] dipoles, actually represented by two charges separated by a short distance, have been added to a biaxial GB potential. In each case, different dipole alignments were investigated. Interesting, and complicated, effects on the phase diagram were seen, particularly on the relative stability of N, Sm, and N_b phases. Generally, for the central dipole, changing its magnitude had more dramatic consequences than changing its direction. The incorporation of the dipole did not seem to increase the range of N_b in these studies, due to increased stabilization of side-by-side arrangements, leading to Sm ordering. Similar conclusions were reached for most of the off-centre arrangements studied; however it was found that if the dipole is shifted along the long molecular axis, and provided it is not too strong, the range of the N_b phase can be extended, and moved towards low temperature.

In principle, a mixture of rodlike and platelike particles may exhibit a N_b phase, but early simulations [226] showed that this is at best highly restricted by demixing. Since that time, there has been little evidence of the N_b phase in mixtures of hard particles. However, the inclusion of attractive interactions in a mixture of hard spherocylinders and cut spheres [227] gave convincing evidence of N_b and SmA_b phases. A mixture of GB molecules may be used to obtain the N_b phase at relatively low temperature [228, 229], while suppressing the tendency to form Sm or Col phases. It seems that

a certain degree of shape dispersity slightly destabilizes the uniaxial N phase and strongly reduces the tendency to form layers, thereby extending the N_b range. However, higher shape dispersity also tends to produce phase separation.

6. Chiral phases

Chiral nematic (N^*) phases, in which the director is perpendicular to the chiral axis, and rotates about it through space, are characterized by their *pitch*: the distance along the axis corresponding to one complete director rotation. Typically pitches are much longer than the practical limits imposed by the box size in molecular simulations. Twisted periodic boundaries [230] may be used to fit one quarter, or one sixth, of the pitch within the box, and such an approach has been used to study twist grain boundaries in the SmA^* phase [231]. Nonetheless, to access the N^* chiral pitches of experimental interest in many cases would require excessively large simulation boxes, and correspondingly long equilibration times.

However, it was soon established that the equilibrium pitch may be calculated indirectly. Firstly, it was shown that the helical twisting power of dopants in a N phase, which relates the pitch to the dopant concentration, could be determined via the difference of chemical potentials between enantiomeric forms, in a twisted nematic [232]. Surprisingly good agreement with experiment was obtained by applying this method to atomistically modelled dopants in a GB solvent [233]. Recent simulations of chiral ruthenium metal complexes in the N phase of N-(4-Methoxybenzylidene)-4-butylaniline (MBBA) and 5CB, with a force field based on GAFF [234–236] use a simpler approach: orientational order parameters are measured, and then used in a surface chirality theory for the helical twisting power.

Subsequently, a route to measuring the pitch, for bulk chiral systems, through intermolecular torque measurements in untwisted and twisted configurations was proposed [237, 238] and applied to a GB(3,5,1,3) system supplemented by a chiral interaction term [239]; results were obtained over a wide range of chiral strengths [240]. Recently, rods composed of fused WCA atoms decorated with a helix of repulsive Yukawa screened charges have been studied in this way [241]. The handedness was shown to change (pitch inversion) on varying the packing fraction, and the strength of chirality of the interactions. A direct approach is also possible, in which the system is confined between two well-separated planar walls, allowing any value of the pitch to develop [242]. This has subsequently been applied to hard spherocylinders with a chiral dispersion potential [243], and to the chiral GB model mentioned above, with an added longitudinal dipole [244]. Hard spherocylinders, decorated in the same manner as Ref. [241], have been studied in a set of self-determining boundaries with soft walls [245]; once again, a pitch inversion was seen.

Recently a purely hard-particle model, a twisted triangular prism, has been shown to exhibit N^* and N^*_D phases, for appropriate shape parameters [246]. This work predominantly used conventional periodic boundaries (with adjustable box dimensions to match the pitch), but also employed both twisted periodic boundary conditions and hard walls as a check. This study makes clear that ascribing a single parameter to quantify molecular 'chirality' is a nontrivial matter.

Molecules formed of helical chains of hard spheres or WCA atoms have been simulated in conventional periodic boundaries with adjustable dimensions [247–250] and with planar walls [251] allowing long-pitch structures to develop. Both a conventional N^* phase, and a novel 'screw-like' N^*_S phase, are seen. In the latter, the molecular short

axis twists around the primary director. The pitch of the phase coincides with that of the constituent molecules, i.e. it is much shorter than that of the conventional N^* phase. A screw-Sm phase is also observed. Phase behaviour, structure, and the unique screw-like diffusion mechanism, were investigated. Recently, the orientational ordering of solutes in both N^* and N_S^* phases has been simulated, to investigate a possible route to distinguishing between enantiomers [252].

Attempts have been made to simulate the chiral twist–bend phase, using achiral bent-core molecules modelled as GB dimers [253] and with the atomistic polarizable force field [190] modelling a cyanobiphenyl dimer [254]. The latter study was complemented by extensive experimental investigation. Rigid achiral curved chains of WCA atoms [255] have also been simulated, giving evidence of the twist–bend phase. The optimized GAFF-LCFF atomistic force field has been used to model emergent chirality in bent-core systems [199, 256], the latter study also involving extensive simulations with a soft spherocylinder model.

7. Interfaces and confined systems

Even for the simplest N phase, the interaction with a planar interface (such as a solid) can give a rich variety of behaviour. For a planar surface, different types of *anchoring* may be distinguished, such as homeotropic (director normal to the surface), planar (director tangential to the surface, but with no specific preferred direction) or homogeneous, and possibly pretilted (in a preferred direction). The anchoring strength measures the resistance, in terms of a mesoscopic free energy, of the surface-induced director orientation to the torque resulting from a deformation of the director in the bulk. Tuning these parameters, by designing or modifying the surface, is a key aspect in technological applications such as switching. Therefore, understanding their microscopic origin has long been a target of molecular simulations. Similar issues arise at the N–vapour interface, and at the equilibrium N–I interface. On top of this, the behaviour of liquid crystals in confined geometry is interesting in its own right, as is the case for isotropic liquids. Finally, colloidal suspensions of nanoparticles in liquid crystals generate interesting defect structures, creating effective inter-particle interactions, with implications for self assembly.

7.1. Equilibrium interfaces and droplets

Early simulations of rigid rod-like particles [257–265] established that planar anchoring is preferred at the equilibrium N–I interface, obtained estimates of the interfacial tension, and studied capillary wave fluctuations. A few GB parametrizations have been shown to exhibit N–vapour coexistence [266–268] with planar or homeotropic anchoring. Recently, this interface has been studied for several GB prolate and oblate models [269], yielding estimates of anchoring strengths and surface tensions. Generally, planar anchoring was observed for those systems having $\kappa > \kappa'$, and homeotropic anchoring otherwise, for both prolate and oblate cases.

Nematic droplets in equilibrium with vapour have been studied for GB(κ,κ',2,1) with $\kappa = 3, 4, 6$ and low values of κ' [270] and for GB(3,1.25,2,1) [271]. In all cases, planar anchoring was seen at the interface; nonspherical, elongated, droplets resulted, with a bipolar director structure and boojum defects located at the ends of the major axis. For the large droplets studied in Ref. [271], a chiral director field developed spontaneously; the nanodroplet extremities became somewhat blunt and the length-

to-width ratio decreased with increasing droplet size, in this regime. This reflects the balance between elastic free energy and surface tension.

Droplets of discotic GB(κ,κ',2,1) molecules, with $\kappa = 0.3, 0.5$ and various κ', have also been studied recently [272]. Droplet shape and director texture depended on the potential parameters. Almost spherical drops with homogeneous director field, and also a bipolar field with tangential anchoring, were seen. On increasing the anisotropy of the energy term κ' in the potential, lens-shaped drops could be generated, or alternatively a spherical shape with homeotropic anchoring and an equatorial disclination ring.

A notable study of the free N surfaces of 5CB and 8CB has combined MD simulations using the force field of Ref. [180], with X-ray reflectivity measurements [273]. Normal alignment was observed, with Sm layering near the surface; this penetrated much further into the bulk N in the 8CB case. Quantitative agreement was found between experiment and simulation.

Finally, freely suspended Sm films have been simulated using models based on soft spherocylinders [274, 275] and using the united-atom model of 8CB [276]. The latter case showed a similar bilayer structure to that seen in the bulk SmA_d phase.

7.2. Planar geometry

Early simulations [277, 278] investigated in some detail the system of hard spherocylinders with $L/\sigma = 15$ in contact with hard walls, establishing the nature of the alignment (both uniaxial and biaxial in the surface phase), the wetting behaviour, and the existence of a capillary nematization transition for wall separations greater than about two molecular lengths. Subsequently, a large number of simulations have been conducted of most of the rigid-particle models mentioned in section 2, in planar geometry. The confined hard spherocylinder system with $L/\sigma = 10$ has been examined recently [279], concentrating on the calculation of the wall–fluid surface tension, and the surface-induced ordering. Ref. [279] also reviews much of the earlier literature in the field, as well as many methodological details. Spherocylinders with $2 \leq L/\sigma \leq 5$ between hard walls [280, 281] show a confinement-induced N phase and an anchoring transition; surface alignment has been studied for hard ellipsoids [282], and thin discs [283] in this geometry.

The pear-shaped model of Ref. [84] has been studied in confined geometry [284] showing some interesting wall-alignment effects. Mixtures of hard spherocylinders with $L/\sigma = 5$ and spheres (up to 20% by number) have been studied between hard parallel walls, initially as a way of stabilizing the coexisting system of I and N phases [285] and then to study the effect of the spheres on surface nematization [286].

Following early simulations of GB(3,5,2,1) molecules between planar walls [287], which investigated two different wall attraction strengths, similar choices of wall parameters have been used to simulate two systems with switched μ and ν indices, GB(3,5,1,2) and GB(2,5,1,2) [288]. Shifts in the various phase transitions, and wall-induced stratification, are studied. The SmA phase of GB(4.4,20,1,1) has been studied between planar walls, by free energy calculations incorporating an interesting modification to the periodic boundary conditions [289].

The discotic system GB(0.5,0.2,1,2) has been studied with wall potentials favouring either homeotropic (face-on) or planar (edge-on) anchoring [290]. In bulk, this system shows N_D and Col phases. Wall-induced density oscillations into the bulk, and more extensive effects on order parameter, were observed; for the studied system sizes, N_D is destabilized relative to Col. The system GB(0.345,0.2,1,2) has been studied in the

same geometry, with different strengths of homeotropic anchoring [291].

Following early work on confined semiflexible hard-sphere chains between hard walls [148] there have been some detailed studies of the I–N transition for WCA chains in very narrow pores [292] and also with a range of wall separations and interaction parameters [154, 293–295].

An HGO model, in which the surface anchoring against a hard wall is adjustable between planar and homeotropic [296], has been used to simulate a hybrid cell, having strong homeotropic anchoring on one wall, and planar, bistable, or weakly homeotropic anchoring on the other [297]. The same model has been used to show that various patterned surfaces may be used to control both azimuthal and zenithal angles of tilt in the bulk N phase [298–301]. The LJ potential with anisotropic attraction [25] has also been simulated between hard walls with different anchoring conditions [302–305]. Various aspects, including wetting behaviour and the effect of striped substrates are investigated.

Various attempts have been made to introduce wall microstructure, while retaining a simple mesogen model. GB(3,5,2,1) has been studied between walls consisting of square arrays of spherical interaction sites [306]. By using position- and angle-dependent interactions with each GB unit, varying the wall site density, and also temperature, a switch from planar to normal wall alignment was induced. The same GB model has been confined between the two halves of a model bilayer membrane, with tunable anchoring strength [307]. A large ($\sim 10^6$ particle) GB(3,5,1,3) system has been simulated between parallel walls composed of fixed GB particles arranged to stabilize a twist cell configuration [308]. The formation of the helical structure from an initial uniform alignment across the cell, was observed. Initially, two uniformly aligned domains were formed, the twist developing afterwards from the interface between them. Additionally, some virtual switching experiments were carried out (see section 8.5). Hard spherocylinders have been studied between walls modified by a layer of adsorbed hard spheres [309] or composed of aligned spherocylinders [310]. Semiflexible WCA chains have been studied in the presence of parallel walls composed of similar beads [311]. The walls take the form of a frozen liquid, and in some cases a striped geometry is used to align the chains. The growth of surface-induced order is studied as a function of chain stiffness. Regular, corrugated walls composed of LJ particles have also been studied [295].

Anchoring of liquid crystals on polymer surfaces has long been an area of activity for simulation, one key question being the relative importance of chain orientation and larger-scale surface features such as grooves. For example, the AMBER-based liquid crystal force field [171], has been used to simulate a small system of 5CB in contact with a polyvinyl alcohol surface [312]. Alignment with the substrate was found to be primarily dictated by the chain direction, but could be influenced by very deep grooves. This paper also summarized previous work in the area. More recently, large scale simulations of the united atom model of 5CB [180] combined with a detailed atomistic model of two polymers, polystyrene (PS) and polymethylmethacrylate (PMMA), have been used to study surface alignment on both amorphous and ordered surfaces [313]. Alignment along the PMMA chains, but perpendicular to the PS chains, was observed, in agreement with experiment; thus, chain stretching, and the chemical nature of the polymer, are important factors. The results also support the view that 'rubbing' of the surface to create microgrooves is not needed to promote alignment.

Anchoring on other surfaces is also of interest. The same molecular model [180] has been used to study films ($\sim$ 20 nm thickness) of 5CB in contact with silicon [314] and silica [315]. Homeotropic (normal) anchoring is seen at the free (vacuum)

interface. For silicon, uniform planar alignment is observed at the solid surface, and the director shows a twist–bend deformation across the film. Planar anchoring is also seen for crystalline silica (cristobalite), with enhanced orientational ordering, and for amorphous silica, with a lower order parameter, but a larger persistence length into the bulk. The effects of surface roughness were also studied in this case. These papers include a discussion of problems involved in defining and measuring the anchoring energy as a function of distance from the surface.

Similar width films (~ 25 nm) composed of 5CB molecules between water and vacuum have been studied [316] using the same force field [180]. Once more, a hybrid film is formed, with a splay–bend transition between homeotropic anchoring at the vacuum interface and tilted-parallel anchoring at the water. Anchoring strengths at the interfaces were estimated. Simulations coupled with experiments suggest that some amphiphiles may locally disorder the liquid crystal, dramatically reducing the anchoring strength at this interface [317].

In an attempt to simulate *homeotropic*, rather than planar, alignment at a solid interface, various systems of self-assembled monolayers (mixtures of alkyltrichlorosilanes) on amorphous silica have been investigated [318]. Once more, the united-atom model of 5CB [180] was employed, and film widths ~ 25 nm bounded by a free interface were studied. It proved possible to adjust the composition and morphology of the substrate to generate either planar or homeotropic alignment. The simulations indicated the importance of fine control over the monolayer assembly to obtain the desired alignment.

A number of other studies have been conducted of individual mesogens, monolayers, or highly-confined liquid crystals, using realistic potentials. Insertion of molecules in the *n*CB family in a bent-core liquid crystal monolayer [319] has shed some light on the mechanism of vertical surface alignment. The insertion process appears to involve a complex free energy landscape having metastable minima; the hydrocarbon tails of the mesogens typically became more rigid on insertion, and for the longer molecules, core-first insertion seems to be favoured. Pretilt of monolayers of 5CB on various polyimide surfaces [320] has been investigated, to isolate the effect of biphenyl side chains.

It is convenient to include here simulation studies of liquid crystal layers adsorbed as a droplet or thin film at an interface between two other materials. Langmuir monolayers of various members of the *n*CB family have been simulated at the air–water interface, using the OPLS-AA force field [321–323], focusing on the variation of tilt angles with surface density. Monolayers of bent-core molecules [324–327] have been modelled with OPLS at the water surface. These simulations support experiments aimed at aligning nematogens such as 5CB. Langmuir monolayers of a phenyl-pyrimidine derivative on water have also been simulated [328].

Nematic films of the GB(3,1,2,1) model (which exhibits N–vapour coexistence), along with a film of GB(3,5,2,1) in the I phase, adsorbed on a solid surface composed of spherical atoms, have been studied by MD [329]. Parameters were chosen to make the condensed phases wet the solid, and system sizes up to $\sim 10^7$ molecules were employed. Film undulation was found to lead to dewetting; much of the study focused on comparing the associated morphologies with those seen in experiment. Large N droplets of GB(3,1.25,2,1) have been simulated in contact with walls composed of crystalline or amorphous arrangements of LJ atoms [330]. The wall attraction was tuned to investigate the wetting behaviour. The droplets were typically elongated in shape, with the director field predominantly along the long axis, with boojum defects at the ends. The systems were sufficiently large that contact angles could be estimated directly, and this varied around the contact line between droplet and

surface. Differences between the crystalline and amorphous surfaces could be seen, but not sufficient to affect the essential results.

7.3. Non-planar geometries

Confinement in cylindrical, spherical, and other shaped pores has predominantly been investigated using idealized simulation models. In most cases, the surface generates strong planar anchoring, and the focus has been on the consequences for the phase behaviour, the spatial structure, and single-particle dynamics. For cylinders, orientational ordering along the axis is quite common, while spherical confinement frequently suppresses the ordered phases altogether. For example, GB(4.4,20,1,1) has been studied in cylindrical and spherical pores of different sizes, composed of LJ atoms [331–334] and in smooth-walled cylinders [335]. Hard spherocyinders with $L/\sigma = 15$ have been simulated in spherical cavities of various radii, with strong planar anchoring [336]. Bipolar nematic droplets are seen within the cavity at high densities. A range of different elongations, in cylindrical confinement has been studied [337], revealing N and chiral phases.

Large-scale simulations of semiflexible FENE/WCA chains, for a range of chain lengths and stiffnesses, have been carried out in the N phase in cylindrical confinement [338]. Here, the aim is to study the influence of collective deflection modes (perpendicular to the director) on the nematic order parameter: such modes are not properly accounted for in standard theories. Simulations of such chains have also been carried out in spherical cavities [339–341]. Various structures are observed, including N order with bipolar defects, layers, and a tennis-ball texture.

Only a few discotic systems have been studied in cylindrical geometry. An early simulation of GB(0.345,0.2,1,2) [342], using a wall-potential favouring edge-on anchoring, showed extensive wall-induced layering but was hampered by metastability. The GB(0.2,0.1,2,1) model [343], which showed a $\mathrm{Col_h}$ phase in bulk, exhibited gradual ordering from a para-N phase to Col and eventually $\mathrm{Col_h}$ on cooling in cylindrical confinement, also with edge-on anchoring.

7.4. Nanoparticles in liquid crystals

The defect structures and interparticle interactions, arising from suspensions of nanoparticles in N and other phases, have exciting implications in areas such as photonics [344, 345]. Much of the liquid crystal modelling may be performed at the mesoscale, by minimizing the Frank or Landau–de Gennes free energy, or using lattice models. However, molecular simulations have also played a role.

Early work simply studied the defect structure around a spherical nanoparticle using variants of the GB potential [346, 347]. For homeotropic anchoring, two disclination defect structures were observed: a 'Saturn-ring' around the particle equator and a 'satellite' defect near one of the poles. Systems of 10^6 molecules were needed in the latter case to minimize periodic boundary condition effects on the director field far from the nanoparticle. More recently, a range of anchoring conditions has been investigated using GB and soft potential models [348, 349] and the effects on defect structure of dragging the nanoparticle through the liquid crystal have been studied [350]. Effective interactions between pairs of nanoparticles, due to the distortion of the director field, have been measured [351, 352]. In the latter work it was shown that strong planar anchoring on the nanoparticle surface results in repulsive interactions, while strong

homeotropic anchoring can produce attractions. Entangled defect topologies around a pair of nanoparticles have been investigated [353]. Simulations have also been performed to study the effects of doping a GB liquid crystal with nanoparticles of various shapes (spherical, rod-like and disc-like) [354] and with nanoparticles decorated with GB units to give various shapes and anchoring conditions [355, 356].

Atomistic simulations of related systems are starting to appear. The AMBER force field was used to model 5CB, 8CB, and a fluorinated mesogen, surrounding a pair of parallel carbon nanotubes [357]. A 5CB:8CB mixture, using the model of Ref. [180], was simulated in the presence of a cylinder with homeotropic anchoring [358]. This generates two line defects parallel to the cylinder axis, and molecular segregation is observed in the defect regions, and the layers surrounding the cylinder.

8. Liquid crystal properties: elasticity and dynamics

The orientational elasticity of liquid crystals is key to both their scientific interest and technological usefulness. The Frank elastic constants [4] determine the equilibrium director field, for given boundary conditions, and the energetics of the response to director perturbations: relating them to molecular structure is a key area in which molecular simulation may make a contribution. However, they are only defined in the limit of long wavelength, or small wavenumber k, so extracting them from simulations requires some care. Liquid crystals also exhibit many interesting dynamical features. In the N phase, single-particle diffusion and hydrodynamic flow are more complex than in isotropic liquids: the reduced symmetry plays an obvious role, and the fact that the director orientation is a slow variable, coupling to the velocity field, introduces completely new effects and transport coefficients. The switching process in N cells is also of interest. In the Sm and Col phases, the simple diffusive model may not apply to single-particle motion. Molecular simulations have recently been applied to all of these areas.

8.1. Elastic properties and flexoelectricity

Early simulations established a method for calculating Frank elastic constants in the N phase by measuring equilibrium director fluctuations as a function of wave-vector [359]. The advantage of this method is that the relevant quantities are calculated simultaneously at all wave-vectors of interest, so the expected low-k behaviour may be confirmed, and an extrapolation to $k \to 0$ performed in a controlled way. Inevitably, though, the simulation system box size L imposes a lower limit $k_{\min} = 2\pi/L$, and also simulation run times must be extended significantly since the relevant relaxation takes place on a timescale $\propto L^2$. Subsequent work has checked these points in detail [360, 361], studying up to 512000 molecules using various GB potentials. Additionally, it has been possible to compare simulation results with theoretical predictions and experimental results for colloidal suspensions of platelike particles, by simulating thin and thick hard discs [362, 363]. Recent large-scale simulation studies of FENE/WCA chains were already mentioned in section 3, and these include calculation of the elastic constants [155] using the fluctuation method. A pronounced dependence of K_2 and K_3 on chain length was found, contrary to theoretical predictions but in accord with experiment.

Different approaches, using free energy perturbations [364] and expanded ensembles [365] have been applied to GB models, and to the united atom model [180] of 5CB [366].

The K_2 twist constant may also be measured by applying a uniform twist, through the periodic boundary conditions, and calculating averages of a function involving intermolecular torques [230, 238, 240]. Finally, a method has been proposed and tested [367] based on averages, and fluctuations, of orientational derivatives of the potential energy, in the untwisted N phase.

A few attempts have been made to simulate the flexoelectric coefficients e_{11} and e_{33}. The longitudinal polar ordering of pear- or wedge-shaped particles in the N phase may couple to a nonvanishing splay deformation through e_{11}; transverse polar ordering of banana-shaped particles may couple to a bend deformation through e_{33}. Early studies combined GB and LJ units to give a pear-shaped molecule. The route to e_{11} proceeded by estimating the direct correlation function [368] or by calculating correlations between polarization and orientational stress [369]. Rigid and semiflexible bent-core molecules, composed of chains of repulsive spheres, have been used to estimate both e_{11} and e_{33} through the correlation route [370], with some caveats regarding run length. A similar approach has been used for an atomistic model of *n*-4-(trans-4-n-pentylcyclohexyl)benzonitrile, PCH5 [371]. Another example uses bent GB dimers in coaxial cylindrical boundaries [372] to apply a fixed bend deformation and measure the response in molecular orientations. More recently, approximate estimates of both flexoelectric coefficients and elastic constants have been made on the basis of a calculation of the direct correlation function, albeit neglecting its angular dependence [373, 374].

8.2. Molecular motion in smectics

Early papers on molecular motion in the SmA phase focused on the possible role of transverse interlayer particles in the mechanism of end-over-end rotation [375] (the so-called 'parking lot mechanism') and on the analysis of layer-to-layer motion as diffusion in an effective potential [376]. It also became clear that interlayer diffusion may be enhanced by screw dislocations [377] which are essentially absent from systems of the size typically studied by molecular simulation.

Stiff nine-bead WCA rods have been simulated by MD in the SmA phase alone or in a mixture with spheres [378–380]. The spheres mostly populate the interlayer regions. Translation of rods between layers was analysed in terms of 'fast' single particles, and although consideration was given to a collective chain-like diffusion mechanism, it was concluded that this did not apply for the rods. Instead, a local 'nematization' around the moving rod was suggested. Rotational motion, via the two-step parking-lot mechanism, in which rods move briefly into the interlayer region, was seen in all the systems, and was significantly facilitated by the presence of the spheres. The sphere diffusion was found to be isotropic. For mixtures of WCA-SC particles of various elongations, with spheres, simulated using Brownian dynamics in the Sm phase [381] the sphere diffusion is anisotropic: intralayer diffusion is faster than interlayer transport. The latter process involves transitory cage formation. At higher mole fractions of spheres, the diffusion shows a collective nature: a single sphere may insert into a rod layer, and open a channel for further transfer.

Simulations of hard spherocylinders of various elongations L/σ in the SmA phase, using MC with small moves to mimic Brownian motion, suggest that stringlike clusters play a role in this system [382–384]. The analogy is made with the dynamical heterogeneities observed in out-of-equilibrium supercooled liquids: slow particles 'rattle' around their layer positions, while fast particles 'jump' to neighbouring layers. Molec-

ular diffusion in the Sm phase of perfectly aligned spherocylinders [385] and WCA-SC particles [386] has also been studied, without reporting any evidence of such clusters.

Single-molecule translocation in smectics has been examined in some detail for the CG model of the azobenzene 8AB8 discussed in section 4 [387, 388]. Attention is paid to both the direct and parking-lot mechanisms, calculating free energy profiles, and a variety of time correlation functions and probability densities. Molecular flexibility plays an important role. A significant conclusion is that the timescale difference between atomistic and CG models is due to (at least) two different effects: a general speedup for CG due to smoother free energy landscapes, and a change in the relative importance of different translocation mechanisms. This illustrates a serious challenge in mapping time scales between these types of model, in general.

8.3. Molecular motion in confined nematics

String-like assemblies have been implicated in the enhanced diffusion observed in MD simulations of the 'reentrant nematic' (RN) phase, confined between smooth walls [389–391]. The phase is termed 'reentrant' because it is typically formed from a translationally more ordered phase such as SmA on lowering the temperature, or raising the pressure. The phase is characterized by a very high orientational order parameter. The simulations used a model combining a WCA-SC shape with a GB-like orientation-dependent interaction energy. Confined GB(3,5,2,1) molecules also show some enhancement of diffusion parallel to the walls, in the near-wall region [392], as do isotropic liquids.

8.4. Molecular motion in columnar phases

Diffusion in a binary mixture of aligned hard spherocylinders of different elongations, chosen to favour the $\mathrm{Col_h}$ phase over Sm [393], and the $\mathrm{Col_h}$ phase of hard oblate spherocylinders [394] has been studied by MC. Similar to the interlayer motion in smectics, diffusion perpendicular to the columns was interpreted in a rattle-and-jump picture, with three different time scales; at the intermediate time scale, where particles feel caging effects due to their surroundings, there is significant departure from Gaussian diffusive behaviour. Significant caging is demonstrated at higher densities. A large-scale simulation of GB(0.345,0.2,1,2) [395] investigated diffusion in the $\mathrm{N_D}$ and Col phases. In the latter case diffusion is strongly influenced by interdigitation and its relaxation, and various modes are identified: rattling, hopping (across columns) and drifting (along the director), with the possibility of hopping involving string-like motion.

8.5. Collective motion in nematics

Collective transport coefficients, such as viscosities, may be computed in a simulation via well-established equilibrium time correlation functions or by nonequilibrium methods. An extensive series of such simulations using variants of the GB model has been carried out by Sarman and Laaksonen; the ones of most interest here concern nematic viscosities and director rotation. Couette flow using sheared periodic boundary conditions, has been used to measure the Miesowicz viscosities, and the twist viscosity, and to observe flow alignment [396, 397] in the N phase, extending into the SmA. A transition to flow instability was seen close to the N–SmA transition. Non-Newtonian flow

effects have been studied [398, 399]. Planar elongational flow has also been simulated [400]. Biaxial particles composed of GB-like discs have been used to study transport coefficients in N, N_D, and N_b phases [401].

The rotational viscosity coefficient γ_1 is of particular interest, in understanding the switching behaviour in nematics. Field-induced director alignment provides a direct route, and has been illustrated for the GB(4.4,20,1,1) model [402]. However, coupling a large external field to a flexible, atomistic, model may produce unwanted side-effects. An alternative is to use equilibrium simulations to calculate γ_1 via the director angular velocity correlation function or angular mean-squared displacement [403], and Ref. [404] gives an example for an atomistic model, together with references to earlier work. The method has been applied, using GAFF, to estimate γ_1 for mixtures of 5CB and 10CB [405], and recently for various fast-response liquid crystal molecules [406]. In this last case, it was concluded that over-emphasis of attractions in the force-field affected the comparison with experiment. Additional approximations may be used to relate γ_1 to single-particle rotation, and this approach has been applied to a variety of atomistically modelled nematics [407, 408].

Wave-vector dependent collective orientational time correlation functions, and their coupling to the hydrodynamic fluid velocity field, have been studied by large-scale equilibrium MD using several variants of the GB model [361, 409]. Systems of $\sim 5 \times 10^5$ molecules are required to confirm the scaling of correlation times $\propto k^{-2}$ predicted by hydrodynamic theory [4]. These predictions were confirmed, but the director bend mode, contrary to conventional belief, was shown to be propagating (oscillatory). This is due to the strength of the coupling coefficient α_2 between director and velocity fields, compared with the geometric mean of the relevant Miesowicz viscosity η_2 and the rotational viscosity γ_1. It was argued that there exists an experimentally realizable range of parameters in which this might be observed, but it is also possible that the simplicity of this type of model (smooth, rigid, uniaxial) results in an unphysically low viscosity, a point also made in relation to γ_1 in Ref. [402].

Collective, low-k, director fluctuations have interesting consequences for single-molecule rotations: a strong long-time tail, proportional to $t^{-1/2}$, is predicted to occur for appropriate components of the orientational correlation function. These have been studied for GB(3,5,2,1) and GB(3,5,1,3) in the N phase [410]. Very large systems are required to offset the effects of periodic boundary conditions which impose a lower limit on k. Good agreement with the predicted behaviour, including the expected finite-size effects, was found, as shown in Fig. 5.

Semiflexible LJ chains have been used in studies of flow alignment in the N phase, and the effect of shear flow on the I–N and I–SmA transitions [411–413]. In these simulations, a mesoscale technique is used to model the solvent hydrodynamically. An interesting phenomenon is observed in a N film bounded by flow-aligned I liquid: with the interfaces lying in the planes defined by the flow and vorticity vectors, the director tilts over and then rotates in this same plane. This involves symmetry breaking, so both clockwise and anticlockwise rotation are seen, successively.

Rigid linear LJ atom chains, confined between rigid walls also composed of LJ atoms, have been simulated with MD [414–416] to study lubrication in flow in the N phase. The dependence of the surface friction coefficient and slip length on the degree and direction of ordering, and on the structure and attractiveness of the walls, have been examined.

GB(κ,1,2,1) models, with $\kappa = 3$–5, have been simulated between parallel walls, under the influence of an electric field, taking into account the interactions between induced dipoles [417, 418]. The aim is to study the generation of backflow: an S-shaped velocity

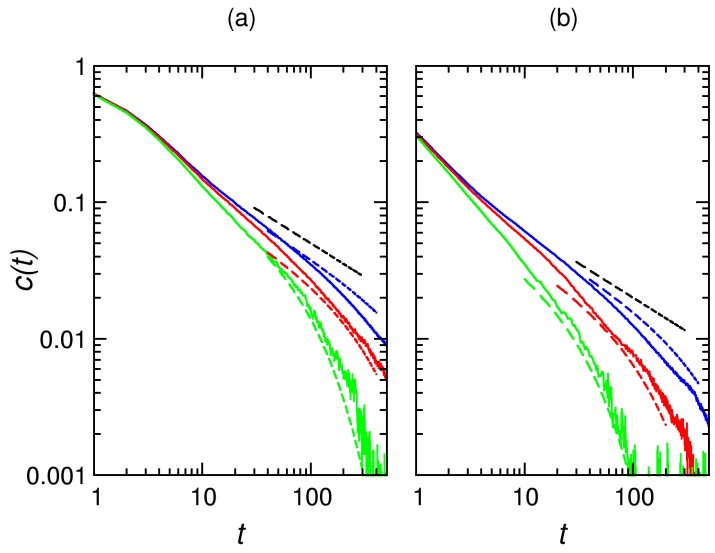

Figure 5. Orientational correlation functions plotted on a log–log scale for (a) GB(3,5,2,1) and (b) GB(3,5,1,3) in the N phase. Solid lines correspond to simulation results for different system sizes, from low to high on the plot: $N = 8000$ (green), $N = 64000$ (red) and $N = 512000$ (blue). Error bars have been omitted for clarity. Dashed lines are guides to the corresponding theoretical long-time tail $\propto t^{-1/2}$, modified by the expected finite-size effect in each case. The uppermost (black) dashed line is for infinite system size. The vertical position of these guide lines is arbitrary; they have been offset slightly for clarity. Adapted by permission of Springer Nature from Fig. 4 of A. Humpert, A.J. Masters, and M.P. Allen, *Eur. Phys. J. Spec. Topics,* **225,** 1723, copyright (2018) [410]; permission conveyed through Copyright Clearance Center, Inc.

profile is observed following application of the reorienting field. The interesting feature of fast switching by rotation about the long axis of a biaxial GB molecule has been simulated directly [419]. The same type of model has been studied in slab geometry [420] between walls composed of uniaxial GB particles. Field-on switching, and field-off relaxation, were simulated with respect to both the primary and secondary directors, with some interesting differences, and correlations, observed, along with the possibility of generating transient and long-lived metastable structures.

9. Ionic liquid crystals

In recent years, liquid crystals composed of charged mesogens have become of great interest, paralleling the growth of research into room-temperature ionic liquids. A comprehensive review has appeared recently [421]. The core of such molecules typically consists of charged imidazolium rings; to these are attached long alkyl chains. Mesophases (Col or Sm) may show highly anisotropic conductivity (in one or two dimensions, respectively). There is the possibility of simulating these materials using CG models, as well as in atomistic detail. It is convenient to also discuss in this section simulations of charged nonspherical particles intended to model colloidal suspensions and clays.

In a 1:1 mixture of centrally, oppositely, charged spherocylinders with $L/\sigma = 5$ [422, 423], N, SmA and SmB phases were observed. Ion pairing is found to reduce the range of the N phase, compared with the uncharged system, in a similar way to what is seen for systems with longitudinal dipoles. A 1:1 mixture of charged spherocylinders

with $L/\sigma = 5$ and oppositely charged, small, hard spheres has been investigated [424]. Two models were examined, respectively with the charge located at the centre of the spherocylinder, giving rise to N and $\mathrm{Col_h}$ phases, or near one end of the spherocylinder, giving N and SmA phases. This difference is influenced by the preferred location of the spherical counter-ions.

Centrally charged GB(4.4,20,1,1) [425, 426], and GB(3,5,1,3) [427] molecules have been simulated in mixtures with oppositely charged LJ ions for a range of charges and state points. By tuning the relative strength of electrostatic and attractive van der Waals interactions, different phases, including ionic N and Sm, may be stabilized. The former is somewhat rare in reality, possibly because molecules such as imidazolium derivatives have some amphiphilic character, which tends to stabilize Sm layers (see below).

A model based on the (prolate) GB potential, with a pair of equal charges symmetrically located on the axis, has been simulated [428]. Solvent counterions are treated implicitly, and a screened Coulomb potential is employed. A 'wide SmA' phase, containing a significant fraction of transverse inter-layer molecules, is reported.

A 1:1 mixture of oppositely, centrally, charged oblate GB-like molecules [110] with $\kappa = 0.5$ has been studied [429]. A transition from N to a charge-ordered SmA phase is seen: discs carrying the same charge occupy the same layers.

An effective screened Coulomb or Yukawa potential, sometimes derived from Poisson–Boltzmann theory [430, 431] with an implicit solvent, has been used in several studies of charged plate-like particles, to model clay suspensions. Charged cut spheres [432] and thin hard disks [433, 434] have exhibited N and $\mathrm{Col_h}$ phases. For the thin disks a novel intergrowth texture consisting of alternating nematic and antinematic layers has also been reported. Plate-like particles composed of WCA LJ units, with charges distributed in a way that distinguishes between edge sites and interior sites, have also been simulated in implicit solvent using a screened Coulomb potential [435–437]. A rich phase diagram including N, Sm, and Col phases, emerges.

A CG force field developed for ionic liquids [438, 439] has been applied to MD simulations of the liquid crystal 1-hexadecyl-3-methylimidazolium nitrate [440, 441]. A SmA phase is seen, apparently stabilized by some microphase segregation between ionic and hydrophobic regions, similar to lipid bilayers [442]. Transition temperatures, however, only agree moderately with experiment. The same model has been used to study the effects of side-chain length [443]. A fully atomistic simulation of the same system has been carried out recently [444], as well as a study of the distribution and diffusion of dissolved Xe atoms [445, 446]. Three homologues of the same molecule have been studied recently using the atomistic OPLS-AA force field, again showing an ionic Sm phase [447]. It should be noted that explicit polarization effects are omitted from the atomistic, and CG, force fields mentioned above. Some MD simulations of imidazolium derivatives using a polarizable force field [190] have been carried out in conjunction with X-ray diffraction [448] to investigate the influence of counterions on interdigitation in the Sm phase.

10. Charge transport in mesophases

The electronic properties of conjugated π-systems have proven useful in the development of a range of technological devices, including solar cells and light emitting diodes. Liquid crystalline systems offer the possibility of combining orientational order with ease of processing and self healing. In particular, disk-like molecules consisting

of an extended aromatic core with attached flexible aliphatic side chains may form Col phases with interesting electronic properties. To investigate these in a simulation, a combination of at least three computational techniques is typically needed: (i) molecular electronic structure is computed via quantum chemistry; (ii) atomic level MD is carried out, typically of a few hundred molecules, to obtain the global and local arrangement of molecules in the mesophase; (iii) a kinetic MC simulation model of charge transport is constructed, based on the information obtained from the MD. There is the possibility of using CG models for the MD, but this carries some dangers, since the charge-transport will be quite sensitive to details of both structure and dynamics.

For example, hexabenzocoronene derivatives have been modelled with AMBER-OPLS potentials and OPLS-AA for the aromatic cores [449–451], studying the dependence of phase behaviour on side chain length. A synthetic molecule, based on the hexabenzocoronene core, has also been simulated using GAFF [452]: the resulting morphologies were used to calculate charge transfer integrals and other necessary information for a kinetic MC scheme to compute the charge mobility. Another family of molecules is the hexakis-n-alkoxy-triphenylenes (HATn), studied in prototype form in a single column [453] and by MD with $N = 72$ molecules [454] to examine the distribution of core–core distances, in support of scattering experiments.

Columnar phases are not the only ones of interest. The biaxial GB potential has been used [455] to study N and Sm phases; structural information from the simulations was used as input to a hopping model for carrier transport. Atomistic simulations of indenofluorene trimers in the Sm phase [456], which agreed well with experimental structures, were used in a kinetic MC scheme to model exciton diffusion. Unexpectedly, the reduction in order parameters on increasing the temperature was found not to influence the measured diffusion length, although the transport was found to be highly anisotropic in the Sm phase.

11. Conclusions

In common with other areas of molecular simulation, the modelling of liquid crystals has benefitted enormously from the steady increase in computer power over the last 35 years. Resources are now sufficient to allow atomistic simulations to investigate the phase diagrams, and static and dynamic properties, of specific systems, comparing directly with experiment. Indeed, a gratifying feature of the last few years has been the increasing number of publications in which experiment and simulation are used in a coordinated way. This has focused attention onto the accuracy of available force fields, and it has become clear that it is still a challenge to reproduce all the properties of interest, although substantial refinements have been made in recent years.

As in other areas of soft condensed matter, multiple timescales and length scales are of interest for liquid crystals. This review has hardly touched on mesoscale simulation approaches, but there seems to be plenty of scope for combining atomistic or molecular modelling techniques with mesoscopic simulation methods, particularly when the evolution of defect structures or domain boundaries is of interest. However, matching the timescales between different levels of modelling can be a serious problem, and one example of this (rotation in Sm phases) was already highlighted above. Charge-transport processes involving liquid crystals have also been modelled by a combination of techniques, albeit in a sequential way; it will be interesting to see if a more integrated approach is feasible.

It seems that simulations of idealized molecular models still have a role to play, as il-

lustrated by recent progress in understanding the stability of the biaxial nematic phase and the continuing interest in understanding chiral phases. Experiments on colloidal suspensions continue to act as a stimulus in this area. Also, although this review has not attempted to discuss theoretical approaches, the close comparison between simulations using simple nonspherical particles, and density functional theory applied to the same models (the legacy of Onsager) clearly continues to illuminate the field.

Acknowledgements

The author would like to take this opportunity to thank the many students, postdoctoral researchers, and colleagues who have inspired him to work in this field over the years. Special thanks also go to the organisers of innumerable summer schools, workshops, and similar events which the author attended, initially as a student and later as a lecturer. The comments of the anonymous referees are gratefully acknowledged.

References

[1] T.J. Sluckin, D.A. Dunmur and H. Stegemeyer, editors, *Crystals That Flow* (CRC Press, London, 2004).
[2] M.P. Allen and D.J. Tildesley, *Computer simulation of liquids*, 2nd ed. (Oxford University Press, Oxford, 2017).
[3] D. Frenkel and B. Smit, *Understanding molecular simulation: from algorithms to applications*, 2nd ed. (Academic Press, San Diego, 2002).
[4] P.G. de Gennes and J. Prost, *The Physics of Liquid Crystals*, 2nd ed. (Clarendon Press, Oxford, 1995).
[5] C. Zannoni, J. Mater. Chem. **11**, 2637–2646 (2001).
[6] C.M. Care and D.J. Cleaver, Rep. Prog. Phys. **68**, 2665–2700 (2005).
[7] M.R. Wilson, Int. Rev. Phys. Chem. **24**, 421–455 (2005).
[8] G.R. Luckhurst, Liq. Cryst. **33**, 1389–1395 (2006).
[9] M.R. Wilson, Chem. Soc. Rev. **36**, 1881–1888 (2007).
[10] C. Zannoni, Liq. Cryst. **45**, 1880–1893 (2018).
[11] D. Andrienko, J. Molec. Liquids **267**, 520–541 (2018).
[12] E.R. Soule and A.D. Rey, Molec. Simul. **38**, 735–750 (2012).
[13] P.A. Lebwohl and G. Lasher, Phys. Rev. A **6**, 426–429 (1972).
[14] A. Antipova and C. Denniston, Soft Matter **12**, 1279–1294 (2016).
[15] T.N. Shendruk and J.M. Yeomans, Soft Matter **11**, 5101–5110 (2015).
[16] A.L. Rabinovich and A.P. Lyubartsev, Polymer Science Ser. C **55**, 162–180 (2013).
[17] A. Masters, Liq. Cryst. Today **25**, 30–37 (2016).
[18] J.M. Ilnytskyi, M. Saphiannikova, D. Neher and M.P. Allen, in *Liquid Crystalline Polymers*, edited by Vijay Kumar Thakur and Michael R. Kessler, Vol. 1 (Springer International Publishing, Switzerland, 2015), pp. 93–129.
[19] J.D. Weeks, D. Chandler and H.C. Andersen, J. Chem. Phys. **54**, 5237–5247 (1971).
[20] P. Tian, D. Bedrov, G.D. Smith and M. Glaser, J. Chem. Phys. **115**, 9055–9064 (2001).
[21] P. Tian and G.D. Smith, J. Chem. Phys. **116**, 9957–9963 (2002).
[22] F. Yan, C.A. Hixson and D.J. Earl, Soft Matter **5**, 4477–4483 (2009).
[23] M.R. Wilson, P.D. Duncan, M. Dennison and A.J. Masters, Soft Matter **8**, 3348–3356 (2012).
[24] K. Kremer and G.S. Grest, J. Chem. Phys. **92**, 5057–5086 (1990).
[25] S. Hess and B. Su, Z. Naturf. A **54**, 559–569 (1999).
[26] M. Greschek and M. Schoen, Phys. Rev. E **83**, 011704 (2011).
[27] L. Onsager, Ann. N. Y. Acad. Sci. **51**, 627–659 (1949).

[28] J.F. Lutsko, Adv. Chem. Phys. **144**, 1–92 (2010).
[29] R. Evans, M. Oettel, R. Roth and G. Kahl, J. Phys. Cond. Mat. **28**, 240401 (2016).
[30] B.J. Alder and T.E. Wainwright, J. Chem. Phys. **27**, 1208–1209 (1957).
[31] W.W. Wood and J.D. Jacobson, J. Chem. Phys. **27**, 1207–1208 (1957).
[32] J.P. Hansen and I.R. McDonald, *Theory of simple liquids with applications to soft matter*, 4th ed. (Academic Press, London, 2013).
[33] J. Vieillard-Baron, J. Chem. Phys. **56**, 4729–4744 (1972).
[34] J. Vieillard-Baron, Molec. Phys. **28**, 809 (1974).
[35] D. Frenkel and R. Eppenga, Phys. Rev. Lett. **49**, 1089–1092 (1982).
[36] R. Eppenga and D. Frenkel, Molec. Phys. **52**, 1303–1334 (1984).
[37] D. Frenkel, B.M. Mulder and J.P. McTague, Phys. Rev. Lett. **52**, 287–290 (1984).
[38] D. Frenkel and B.M. Mulder, Molec. Phys. **55**, 1171–1192 (1985).
[39] H. Miao, Y. Li, S. Li, H.G. Xu and H.R. Ma, Chinese Phys. Lett. **32**, 026401 (2015).
[40] S. Heymans and T. Schilling, Phys. Rev. E **96**, 022708 (2017).
[41] U. Agarwal and F.A. Escobedo, Nature Materials **10**, 230–235 (2011).
[42] P.F. Damasceno, M. Engel and S.C. Glotzer, Science **337** (6093), 453–457 (2012).
[43] C. Avendano and F.A. Escobedo, Curr. Opin. Colloid Interf. Sci. **30**, 62–69 (2017).
[44] L. Mederos, E. Velasco and Y. Martinez-Raton, J. Phys. Cond. Mat. **26**, 463101 (2014).
[45] P.E. Brumby, A.J. Haslam, E. de Miguel and G. Jackson, Molec. Phys. **109**, 169–189 (2011).
[46] D.W. Rebertus and K.M. Sando, J. Chem. Phys. **67**, 2585–2590 (1977).
[47] M.P. Allen, D. Frenkel and J. Talbot, Comput. Phys. Rep. **9**, 301–353 (1989).
[48] A. Donev, S. Torquato and F.H. Stillinger, J. Comput. Phys. **202**, 737–764 (2005).
[49] C. De Michele, J. Comput. Phys. **229**, 3276–3294 (2010).
[50] A.T. Gabriel, T. Meyer and G. Germano, J. Chem. Theor. Comput. **4**, 468–476 (2008).
[51] J.W. Perram and M.S. Wertheim, J. Comput. Phys. **58**, 409–416 (1985).
[52] B.J. Berne and P. Pechukas, J. Chem. Phys. **56**, 4213–4216 (1972).
[53] G. Odriozola and F.D. Guevara-Rodriguez, J. Chem. Phys. **134**, 201103 (2011).
[54] F.D. Guevara-Rodriguez and G. Odriozola, J. Chem. Phys. **135**, 084508 (2011).
[55] G. Odriozola, J. Chem. Phys. **136**, 134505 (2012).
[56] D. Frenkel, J. Phys. Chem. **91**, 4912–4916 (1987).
[57] J.A.C. Veerman and D. Frenkel, Phys. Rev. A **41**, 3237–3244 (1990).
[58] P.G. Bolhuis and D. Frenkel, J. Chem. Phys. **106**, 666–687 (1997).
[59] S. Dussi, M. Chiappini and M. Dijkstra, Molec. Phys. **116**, 2792–2805 (2018).
[60] D. Frenkel, Liq. Cryst. **5**, 929–940 (1989).
[61] J.A.C. Veerman and D. Frenkel, Phys. Rev. A **45**, 5632–5648 (1992).
[62] R.P.S. Fartaria and M.B. Sweatman, Chem. Phys. Lett. **478**, 150–154 (2009).
[63] R.P.S. Fartaria, N. Javid, J. Sefcik and M.B. Sweatman, J. Coll. Int. Sci. **377**, 94–104 (2012).
[64] P.D. Duncan, M. Dennison, A.J. Masters and M.R. Wilson, Phys. Rev. E **79**, 031702 (2009).
[65] P.D. Duncan, A.J. Masters and M.R. Wilson, Phys. Rev. E **84**, 011702 (2011).
[66] M. Marechal, A. Patti, M. Dennison and M. Dijkstra, Phys. Rev. Lett. **108**, 206101 (2012).
[67] M. Mathew, T. Schilling and M. Oettel, Phys. Rev. E **85**, 061407 (2012).
[68] T. Schilling, S. Dorosz, M. Radu, M. Mathew, S. Jungblut and K. Binder, Euro. Phys. J. Spec. Top. **222**, 3039–3052 (2013).
[69] A. Atashpendar, S. Arora, A.D. Rahm and T. Schilling, Phys. Rev. E **98**, 062611 (2018).
[70] A. Cuetos and B. Martinez-Haya, J. Chem. Phys. **129**, 214706 (2008).
[71] M. Marechal, A. Cuetos, B. Martinez-Haya and M. Dijkstra, J. Chem. Phys. **134**, 094501 (2011).
[72] B. Martinez-Haya and A. Cuetos, Molec. Simul. **35**, 1077–1083 (2009).
[73] B. Martinez-Haya and A. Cuetos, J. Chem. Phys. **131**, 074901 (2009).
[74] B. Martinez-Haya and A. Cuetos, Phys. Rev. E **81**, 020701 (2010).

[75] F. Gamez, R.D. Acemel and A. Cuetos, Molec. Phys. **111**, 3136–3146 (2013).
[76] T. Kihara, J. Phys. Soc. Japan **6**, 289–296 (1951).
[77] A. Cuetos and B. Martinez-Haya, Molec. Phys. **113**, 1137–1144 (2015).
[78] K.M. Aoki, M. Yoneya and H. Yokoyama, Phys. Rev. E **81**, 021701 (2010).
[79] K.M. Aoki and M. Yoneya, J. Phys. Soc. Japan **80**, 124603 (2011).
[80] K.M. Aoki, J. Phys. Soc. Japan **83**, 104603 (2014).
[81] K.M. Aoki and S. Ohnishi, Mol. Cryst. Liq. Cryst. **612**, 64–71 (2015).
[82] S. Varga and F.J. Vesely, J. Chem. Phys. **131**, 194506 (2009).
[83] F. Gamez and S. Lago, Molec. Phys. **115**, 1186–1190 (2017).
[84] F. Barmes, M. Ricci, C. Zannoni and D.J. Cleaver, Phys. Rev. E **68**, 021708 (2003).
[85] M. Marechal, R.J. Kortschot, A.F. Demirörs, A. Imhof and M. Dijkstra, Nano. Lett. **10**, 1907–1911 (2010).
[86] M. Marechal and M. Dijkstra, Phys. Rev. E **82**, 031405 (2010).
[87] G. Cinacchi and J.S. van Duijneveldt, J. Phys. Chem. Lett. **1**, 787–791 (2010).
[88] G. Cinacchi, J. Chem. Phys. **139**, 124908 (2013).
[89] G. Cinacchi and A. Tani, J. Chem. Phys. **141**, 154901 (2014).
[90] G. Cinacchi and S. Torquato, J. Chem. Phys. **143**, 224506 (2015).
[91] M.A. Bates, M. Dennison and A. Masters, J. Chem. Phys. **129**, 074901 (2008).
[92] D. de las Heras, S. Varga and F.J. Vesely, J. Chem. Phys. **134**, 214902 (2011).
[93] S.D. Peroukidis, Soft Matter **8**, 11062–11071 (2012).
[94] S.D. Peroukidis, A.G. Vanakaras and D.J. Photinos, Phys. Rev. E **91**, 062501 (2015).
[95] J.G. Gay and B.J. Berne, J. Chem. Phys. **74**, 3316–3319 (1981).
[96] M.A. Bates and G.R. Luckhurst, J. Chem. Phys. **104**, 6696–6709 (1996).
[97] M.A. Bates and G.R. Luckhurst, J. Chem. Phys. **110**, 7087–7108 (1999).
[98] R. Berardi, A.P.J. Emerson and C. Zannoni, J. Chem. Soc. Faraday Trans. **89**, 4069–4078 (1993).
[99] E. de Miguel, E. Martín del Río, J.T. Brown and M.P. Allen, J. Chem. Phys. **105**, 4234–4249 (1996).
[100] J.T. Brown, M.P. Allen, E. Martín del Río and E. de Miguel, Phys. Rev. E **57**, 6685–6699 (1998).
[101] G.R. Luckhurst, R.A. Stephens and R.W. Phippen, Liq. Cryst. **8**, 451–464 (1990).
[102] M.P. Allen and G. Germano, Molec. Phys. **104**, 3225–3235 (2006).
[103] R. Berardi, C. Fava and C. Zannoni, Chem. Phys. Lett. **236**, 462–468 (1995).
[104] D.J. Cleaver, C.M. Care, M.P. Allen and M.P. Neal, Phys. Rev. E **54**, 559–567 (1996).
[105] R. Berardi, C. Fava and C. Zannoni, Chem. Phys. Lett. **297**, 8–14 (1998).
[106] R. Berardi, J.S. Lintuvuori, M.R. Wilson and C. Zannoni, J. Chem. Phys. **135**, 134119 (2011).
[107] W.K. Qi, Y. Xu, K.L. Yung and Y. Chen, Polymer **53**, 634–639 (2012).
[108] J. Saha, Phys. Lett. A **375**, 1893–1897 (2011).
[109] J. Saha, Molec. Simul. **42**, 1437–1443 (2016).
[110] R. Everaers and M.R. Ejtehadi, Phys. Rev. E **67**, 041710 (2003).
[111] M. Babadi, M.R. Ejtehadi and R. Everaers, J. Comput. Phys. **219**, 770–779 (2006).
[112] E. de Miguel, Molec. Phys. **100**, 2449–2459 (2002).
[113] C.C. Huang, S. Ramachandran and J.P. Ryckaert, Phys. Rev. E **90**, 062506 (2014).
[114] J.A. Moreno-Razo, O. Cienegas-Caceres, E. Diaz-Herrera and J. Quintana, AIP Conference Proceedings **979**, 120–129 (2008).
[115] C. Bacchiocchi and C. Zannoni, Phys. Rev. E **58**, 3237–3244 (1998).
[116] D. Chakrabarti and D.J. Wales, Phys. Rev. Lett. **100**, 127801 (2008).
[117] K. Satoh, Thin Solid Films **517**, 1411–1416 (2008).
[118] K. Satoh, Mol. Cryst. Liq. Cryst. **516**, 74–80 (2010).
[119] A.P.J. Emerson, G.R. Luckhurst and S.G. Whatling, Molec. Phys. **82**, 113–124 (1994).
[120] M. Ricci, R. Berardi and C. Zannoni, Soft Matter **4**, 2030–2038 (2008).
[121] S.C. McGrother, A. Gil-Villegas and G. Jackson, Molec. Phys. **95**, 657–673 (1998).
[122] M. Houssa, B. Oualid and L.F. Rull, Molec. Phys. **94**, 439–446 (1998).

[123] M. Houssa, L.F. Rull and S.C. McGrother, J. Chem. Phys. **109**, 9529–9542 (1998).
[124] K. Satoh, Mol. Cryst. Liq. Cryst. **480**, 202–218 (2008).
[125] A. Gil-Villegas, S.C. McGrother and G. Jackson, Chem. Phys. Lett. **269**, 441–447 (1997).
[126] R. Berardi, S. Orlandi and C. Cannoni, Int. J. Mod. Phys. C **10**, 477–484 (1999).
[127] S.C. McGrother, A. Gilvillegas and G. Jackson, J. Phys. Cond. Mat. **8**, 9649–9655 (1996).
[128] R. Berardi, S. Orlandi, D.J. Photinos, A.G. Vanakaras and C. Zannoni, Phys. Chem. Chem. Phys. **4**, 770–777 (2002).
[129] M. Houssa, L.F. Rull and J.M. Romero-Enrique, J. Chem. Phys. **130**, 154504 (2009).
[130] T.K. Bose, Phys. Rev. E **98**, 050701 (2018).
[131] R. Berardi, S. Orlandi and C. Zannoni, Phys. Rev. E **67**, 041708 (2003).
[132] T.K. Bose and J. Saha, Phys. Rev. E **86**, 050701 (2012).
[133] T.K. Bose and J. Saha, Phys. Rev. E **89**, 046502 (2014).
[134] N.V. Madhusudana, Phys. Rev. E **89**, 046501 (2014).
[135] M.P. Neal and A.J. Parker, Chem. Phys. Lett. **294**, 277 (1998).
[136] T. Troppenz, L. Filion, R. van Roij and M. Dijkstra, J. Chem. Phys. **141**, 154903 (2014).
[137] T.K. Bose and J. Saha, Phys. Rev. Lett. **110**, 265701 (2013).
[138] T.K. Bose and J. Saha, Phys. Rev. E **89**, 052509 (2014).
[139] T.K. Bose and J. Saha, Phys. Rev. E **92**, 042503 (2015).
[140] J.S.J. Lee, R.O. Sokolovskii, R. Berardi, C. Zannoni and E.E. Burnell, Chem. Phys. Lett. **454**, 56–60 (2008).
[141] R.O. Sokolovskii and E.E. Burnell, J. Chem. Phys. **130**, 154507 (2009).
[142] M. Whittle and A.J. Masters, Molec. Phys. **72**, 247–265 (1991).
[143] D.C. Williamson and G. Jackson, J. Chem. Phys. **108**, 10294–10302 (1998).
[144] A. Yethiraj and H. Fynewever, Molec. Phys. **93**, 693–701 (1998).
[145] C. Vega, C. McBride and L.G. MacDowell, J. Chem. Phys. **115**, 4203–4211 (2001).
[146] B. Oyarzun, T. van Westen and T.J.H. Vlugt, J. Chem. Phys. **138**, 204905 (2013).
[147] M.R. Wilson and M.P. Allen, Molec. Phys. **80**, 277–295 (1993).
[148] F.A. Escobedo and J.J. de Pablo, J. Chem. Phys. **106**, 9858–9868 (1997).
[149] C. McBride, C. Vega and L.G. MacDowell, Phys. Rev. E **64**, 011703 (2001).
[150] B. Oyarzun, T. van Westen and T.J.H. Vlugt, J. Chem. Phys. **142**, 064903 (2015).
[151] G. Cinacchi and L. De Gaetani, Phys. Rev. E **77**, 051705 (2008).
[152] G. Cinacchi and L. De Gaetani, Mol. Cryst. Liq. Cryst. **495**, 626–636 (2008).
[153] B. de Braaf, M.O. Menegon, S. Paquay and P. van der Schoot, J. Chem. Phys. **147**, 244901 (2017).
[154] S.A. Egorov, A. Milchev and K. Binder, Polymers **8**, 296 (2016).
[155] A. Milchev, S.A. Egorov, K. Binder and A. Nikoubashman, J. Chem. Phys. **149**, 174909 (2018).
[156] S.A. Egorov, A. Milchev, P. Virnau and K. Binder, Soft Matter **12**, 4944–4959 (2016).
[157] V. Padmanabhan, S.K. Kumar and A. Yethiraj, J. Chem. Phys. **128**, 124908 (2008).
[158] T. van Westen, B. Oyarzun, T.J.H. Vlugt and J. Gross, J. Chem. Phys. **142**, 244903 (2015).
[159] B.O. Rivera, T. van Westen and T.J.H. Vlugt, Molec. Phys. **114**, 895–908 (2016).
[160] M.R. Wilson and M.P. Allen, Mol. Cryst. Liq. Cryst. **198**, 465–477 (1991).
[161] C. McBride, M.R. Wilson and J.A.K. Howard, Molec. Phys. **93**, 955–964 (1998).
[162] C. Amovilli, I. Cacelli, G. Cinacchi, L.D. Gaetani, G. Prampolini and A. Tani, Theor. Chem. Acc. **117**, 885–901 (2006).
[163] M. Bizzarri, I. Cacelli, G. Prampolini and A. Tani, J. Phys. Chem. A **108**, 10336–10341 (2004).
[164] I. Cacelli, G. Prampolini and A. Tani, J. Phys. Chem. B **109** (8), 3531–3538 (2005).
[165] I. Cacelli, L.D. Gaetani, G. Prampolini and A. Tani, J. Phys. Chem. B **111**, 2130–2137 (2007).
[166] M. Cifelli, L. De Gaetani, G. Prampolini and A. Tani, J. Phys. Chem. B **112**, 9777–9786 (2008).
[167] L. De Gaetani and G. Prampolini, Soft Matter **5**, 3517–3526 (2009).

[168] I. Cacelli, C.F. Lami and G. Prampolini, J. Comput. Chem. **30**, 366–378 (2009).
[169] I. Cacelli, A. Cimoli, L. De Gaetani, G. Prampolini and A. Tani, J. Chem. Theor. Comput. **5**, 1865–1876 (2009).
[170] W.D. Cornell, P. Cieplak, C.I. Bayly, I.R. Gould, K.M. Merz, D.M. Ferguson, D.C. Spellmeyer, T. Fox, J.W. Caldwell and P.A. Kollman, J. Am. Chem. Soc. **117**, 5179–5197 (1995).
[171] D.L. Cheung, S.J. Clark and M.R. Wilson, Phys. Rev. E **65**, 051709 (2002).
[172] W.L. Jorgensen, D.S. Maxwell and J. Tirado-Rives, J. Am. Chem. Soc. **118**, 11225–11236 (1996).
[173] F.Y. Yan and D.J. Earl, Soft Matter **7**, 10266–10273 (2011).
[174] J. Peláez and M. Wilson, Phys. Chem. Chem. Phys. **9**, 2968–2975 (2007).
[175] M.T. Sims, L.C. Abbott, S.J. Cowling, J.W. Goodby and J.N. Moore, Chemistry **21**, 10123–10130 (2015).
[176] M.T. Sims, L.C. Abbott, S.J. Cowling, J.W. Goodby and J.N. Moore, Phys. Chem. Chem. Phys. **18**, 20651–20663 (2016).
[177] M.T. Sims, R.J. Mandle, J.W. Goodby and J.N. Moore, Liq. Cryst. **44**, 2029–2045 (2017).
[178] S.K. Fegan, P. Kirsch and F. Müller-Plathe, Liq. Cryst. **45**, 1377–1384 (2018).
[179] R. Berardi, L. Muccioli and C. Zannoni, ChemPhysChem **5**, 104–111 (2004).
[180] G. Tiberio, L. Muccioli, R. Berardi and C. Zannoni, ChemPhysChem **10**, 125–136 (2009).
[181] M.F. Palermo, A. Pizzirusso, L. Muccioli and C. Zannoni, J. Chem. Phys. **138**, 204901 (2013).
[182] A. Pizzirusso, M.B. Di Cicco, G. Tiberio, L. Muccioli, R. Berardi and C. Zannoni, J. Phys. Chem. B **116**, 3760–3771 (2012).
[183] A.C.J. Weber, A. Pizzirusso, L. Muccioli, C. Zannoni, W.L. Meerts, C.A. de Lange and E.E. Burnell, J. Chem. Phys. **136**, 174506 (2012).
[184] A. Pizzirusso, M.E. Di Pietro, G. De Luca, G. Celebre, M. Longeri, L. Muccioli and C. Zannoni, ChemPhysChem **15**, 1356–1367 (2014).
[185] E. Kuprusevicius, R. Edge, H. Gopee, A.N. Cammidge, E.J.L. McInnes, M.R. Wilson and V.S. Oganesyan, Chemistry **16**, 11558–11562 (2010).
[186] F. Chami, M.R. Wilson and V.S. Oganesyan, Soft Matter **8**, 6823–6833 (2012).
[187] A.J. McDonald and S. Hanna, J. Chem. Phys. **124**, 164906 (2006).
[188] V.S. Oganesyan, Liquid Crystals **45**, 2139–2157 (2018).
[189] J.G. Zhang, J.Y. Su and H.X. Guo, J. Phys. Chem. B **115**, 2214–2227 (2011).
[190] O. Borodin, J. Phys. Chem. B **113**, 11463–11478 (2009).
[191] X.Y. Wei, J.B. Hooper and D. Bedrov, Liq. Cryst. **44**, 332–347 (2017).
[192] A. Pizzirusso, M. Savini, L. Muccioli and C. Zannoni, J. Mater. Chem. **21**, 125–133 (2011).
[193] Y. Olivier, L. Muccioli and C. Zannoni, ChemPhysChem **15**, 1345–1355 (2014).
[194] E.D. Gerts, A.V. Komolkin, V.A. Burmistrov, V.V. Alexandriysky and S.V. Dvinskikh, J. Chem. Phys. **141**, 074503 (2014).
[195] R. Vadnais, M.A. Beaudoin and A. Soldera, J. Chem. Phys. **129**, 164908 (2008).
[196] F. Porzio, E. Levert and A. Soldera, Ferroelectrics **431**, 121–128 (2012).
[197] F. Porzio, E. Levert, R. Vadnais and A. Soldera, J. Phys. Chem. B **118**, 4037–4043 (2014).
[198] N.J. Boyd and M.R. Wilson, Phys. Chem. Chem. Phys. **17**, 24851–24865 (2015).
[199] N.J. Boyd and M.R. Wilson, Phys. Chem. Chem. Phys. **20**, 1485–1496 (2018).
[200] C. Peter and K. Kremer, Soft Matter **5**, 4357–4366 (2009).
[201] M.G. Saunders and G.A. Voth, Ann. Rev. Biophys. **42**, 73–93 (2013).
[202] C. Peter, L. Delle Site and K. Kremer, Soft Matter **4**, 859–869 (2008).
[203] B. Mukherjee, L. Delle Site, K. Kremer and C. Peter, J. Phys. Chem. B **116**, 8474–8484 (2012).
[204] G. Megariotis, A. Vyrkou, A. Leygue and D.N. Theodorou, Ind. Eng. Chem. Res. **50**, 546–556 (2011).

[205] J.G. Zhang, J.Y. Su, Y.P. Ma and H.X. Guo, J. Phys. Chem. B **116**, 2075–2089 (2012).
[206] J.G. Zhang and H.X. Guo, J. Phys. Chem. B **118**, 4647–4660 (2014).
[207] S.P. Ju, S.C. Huang, K.H. Lin, H.Y. Chen and T.K. Shen, J. Phys. Chem. C **120**, 14277–14288 (2016).
[208] G.R. Luckhurst and P.S.J. Simmonds, Molec. Phys. **80**, 233–252 (1993).
[209] C.K. Lee, C.C. Hua and S.A. Chen, J. Chem. Phys. **133**, 064902 (2010).
[210] T. Heinemann, K. Palczynski, J. Dzubiella and S.H.L. Klapp, J. Chem. Phys. **141**, 214110 (2014).
[211] R. Pecheanu and N.M. Cann, Phys. Rev. E **81**, 041704 (2010).
[212] R. Berardi, L. Muccioli, S. Orlandi, M. Ricci and C. Zannoni, J. Phys. Cond. Mat. **20**, 463101 (2008).
[213] M.P. Allen, Liq. Cryst. **8**, 499–511 (1990).
[214] P.J. Camp and M.P. Allen, J. Chem. Phys. **106**, 6681–6688 (1997).
[215] M. Marechal, S. Dussi and M. Dijkstra, J. Chem. Phys. **146**, 124905 (2017).
[216] A. Cuetos, M. Dennison, A. Masters and A. Patti, Soft Matter **13**, 4720–4732 (2017).
[217] A. Patti and A. Cuetos, Molec. Simul. **44**, 516–522 (2018).
[218] S.D. Peroukidis, A.G. Vanakaras and D.J. Photinos, Phys. Rev. E **88**, 062508 (2013).
[219] S.D. Peroukidis and A.G. Vanakaras, Soft Matter **9**, 7419–7423 (2013).
[220] N. Tasios and M. Dijkstra, J. Chem. Phys. **146**, 144901 (2017).
[221] S. Dussi, N. Tasios, T. Drwenski, R. van Roij and M. Dijkstra, Phys. Rev. Lett. **120**, 177801 (2018).
[222] A. Cuetos, E.M. Rafael, D. Corbett and A. Patti, Soft Matter **15**, 1922–1926 (2019).
[223] S. Orlandi, L. Muccioli and R. Berardi, Liq. Cryst. **45**, 2400–2415 (2018).
[224] L. Querciagrossa, M. Ricci, R. Berardi and C. Zannoni, Phys. Chem. Chem. Phys. **15**, 19065–19072 (2013).
[225] L. Querciagrossa, R. Berardi and C. Zannoni, Soft Matter **14**, 2245–2253 (2018).
[226] P.J. Camp, M.P. Allen, P.G. Bolhuis and D. Frenkel, J. Chem. Phys. **106**, 9270–9275 (1997).
[227] A. Cuetos, A. Galindo and G. Jackson, Phys. Rev. Lett. **101**, 237802 (2008).
[228] R. Berardi and C. Zannoni, Soft Matter **8**, 2017–2025 (2012).
[229] L. Querciagrossa, M. Ricci, R. Berardi and C. Zannoni, Phys. Chem. Chem. Phys. **19**, 2286–2294 (2017).
[230] M.P. Allen and A.J. Masters, Molec. Phys. **79**, 277–289 (1993).
[231] M.P. Allen, M.A. Warren and M.R. Wilson, Phys. Rev. E **57**, 5585–5596 (1998).
[232] M.P. Allen, Phys. Rev. E **47**, 4611–4614 (1993).
[233] M.J. Cook and M.R. Wilson, J. Chem. Phys. **112**, 1560–1564 (2000).
[234] G. Watanabe and J. Yoshida, J. Phys. Chem. B **120**, 6858–6864 (2016).
[235] G. Watanabe, A. Yamazaki and J. Yoshida, Mol. Cryst. Liq. Cryst. **647**, 235–243 (2017).
[236] J. Yoshida, S. Tamura, K. Hoshino, H. Yuge, H. Sato, A. Yamazaki, S. Yoneda and G. Watanabe, J. Phys. Chem. B **122**, 10615–10626 (2018).
[237] A.B. Harris, R.D. Kamien and T.C. Lubensky, Phys. Rev. Lett. **78**, 1476–1479 (1997).
[238] M.P. Allen and A.J. Masters, J. Mater. Chem. **11**, 2678–2689 (2001).
[239] R. Memmer, H.G. Kuball and A. Schönhofer, Liq. Cryst. **15**, 345–360 (1993).
[240] G. Germano, M.P. Allen and A.J. Masters, J. Chem. Phys. **116**, 9422–9430 (2002).
[241] S. Ruzicka and H.H. Wensink, Soft Matter **12**, 5205–5213 (2016).
[242] S. Varga and G. Jackson, Chem. Phys. Lett. **377**, 6–12 (2003).
[243] S. Varga and G. Jackson, Molec. Phys. **104**, 3681–3691 (2006).
[244] T. Nozawa, P. Brumby and K. Yasuoka, Int. J. Mol. Sci. **19**, 2715 (2018).
[245] A. Kuhnhold and T. Schilling, J. Chem. Phys. **145**, 194904 (2016).
[246] S. Dussi and M. Dijkstra, Nature Comm. **7**, 11175 (2016).
[247] E. Frezza, A. Ferrarini, H.B. Kolli, A. Giacometti and G. Cinacchi, J. Chem. Phys. **138**, 164906 (2013).
[248] E. Frezza, A. Ferrarini, H.B. Kolli, A. Giacometti and G. Cinacchi, Phys. Chem. Chem. Phys. **16**, 16225–16232 (2014).

[249] H.B. Kolli, E. Frezza, G. Cinacchi, A. Ferrarini, A. Giacometti, T.S. Hudson, C. De Michele and F. Sciortino, Soft Matter **10**, 8171–8187 (2014).
[250] G. Cinacchi, A.M. Pintus and A. Tani, J. Chem. Phys. **145**, 134903 (2016).
[251] G. Cinacchi, A. Ferrarini, A. Giacometti and H.B. Kolli, J. Chem. Phys. **147**, 224903 (2017).
[252] J.G. Bojart, C. D'Urso, G. Celebre and G. Cinacchi, Phys. Rev. E **98**, 042704 (2018).
[253] R. Memmer, Liq. Cryst. **29**, 483–496 (2002).
[254] D. Chen, J.H. Porada, J.B. Hooper, A. Klittnick, Y.Q. Shen, M.R. Tuchband, E. Korblova, D. Bedrov, D.M. Walba, M.A. Glaser, J.E. Maclennan and N.A. Clark, Proc. Nat. Acad. Sci. **110**, 15931–15936 (2013).
[255] C. Greco and A. Ferrarini, Phys. Rev. Lett. **115**, 147801 (2015).
[256] J.S. Lintuvuori, G. Yu, M. Walker and M.R. Wilson, Liq. Cryst. **45**, 1996–2009 (2018).
[257] M.A. Bates and C. Zannoni, Chem. Phys. Lett. **280**, 40–45 (1997).
[258] M.P. Allen, J. Chem. Phys. **112**, 5447–5453 (2000).
[259] M.S. Al-Barwani and M.P. Allen, Phys. Rev. E **62**, 6706–6710 (2000).
[260] A.J. McDonald, M.P. Allen and F. Schmid, Phys. Rev. E **63**, 010701(R) (2000).
[261] N. Akino, F. Schmid and M.P. Allen, Phys. Rev. E **63**, 041706 (2001).
[262] R.L.C. Vink and T. Schilling, Phys. Rev. E **71**, 051716 (2005).
[263] R.L.C. Vink, S. Wolfsheimer and T. Schilling, J. Chem. Phys. **123**, 074901 (2005).
[264] S. Wolfsheimer, C. Tanase, K. Shundyak, R. van Roij and T. Schilling, Phys. Rev. E **73**, 061703 (2006).
[265] F. Schmid, G. Germano, S. Wolfsheimer and T. Schilling, Macrom. Symp. **252**, 110–118 (2007).
[266] A.P.J. Emerson, S. Faetti and C. Zannoni, Chem. Phys. Lett. **271**, 241–246 (1997).
[267] E.M. del Río and E. de Miguel, Phys. Rev. E **55**, 2916–2924 (1997).
[268] S.J. Mills, C.M. Care, M.P. Neal and D.J. Cleaver, Phys. Rev. E **58**, 3284–3294 (1998).
[269] L.F. Rull and J.M. Romero-Enrique, Molec. Phys. **115**, 1214–1224 (2017).
[270] L.F. Rull, J.M. Romero-Enrique and A. Fernandez-Nieves, J. Chem. Phys. **137**, 034505 (2012).
[271] D. Vanzo, M. Ricci, R. Berardi and C. Zannoni, Soft Matter **8**, 11790–11800 (2012).
[272] L.F. Rull and J.M. Romero-Enrique, Langmuir **33**, 11779–11787 (2017).
[273] M. Sadati, H. Ramezani-Dakhel, W. Bu, E. Sevgen, Z. Liang, C. Erol, M. Rahimi, N.T. Qazvin, B.H. Lin, N.L. Abbott, B. Roux, M.L. Schlossman and J.J. de Pablo, J. Am. Chem. Soc. **139**, 3841–3850 (2017).
[274] M. Torikai, J. Phys. Soc. Japan **77**, 074602 (2008).
[275] B. Schulz, M.G. Mazza and C. Bahr, Phys. Rev. E **90**, 040501 (2014).
[276] M.F. Palermo, L. Muccioli and C. Zannoni, Phys. Chem. Chem. Phys. **17**, 26149–26159 (2015).
[277] R. van Roij, M. Dijkstra and R. Evans, Europhys. Lett. **49**, 350–356 (2000).
[278] M. Dijkstra, R. van Roij and R. Evans, Phys. Rev. Lett. **63**, 051703 (2001).
[279] P.E. Brumby, H.H. Wensink, A.J. Haslam and G. Jackson, Langmuir **33**, 11754–11770 (2017).
[280] M.A. Semiromi and A. Avazpour, Liq. Cryst. **45**, 262–269 (2018).
[281] M.A. Semiromi and A. Avazpour, Liq. Cryst. **45**, 1396–1407 (2018).
[282] H. Miao and H.R. Ma, Chinese J. Chem. Phys. **29**, 212–218 (2016).
[283] M. Engelsberg and E.N. de Azevedo, J. Phys. Chem. B **112**, 7045–7050 (2008).
[284] P.W.A. Schoenhoefer, G.E. Schroder-Turk and M. Marechal, J. Chem. Phys. **148**, 124104 (2018).
[285] L. Wu, A. Malijevsky, G. Jackson, E.A. Muller and C. Avendano, J. Chem. Phys. **143**, 044906 (2015).
[286] L. Wu, A. Malijevsky, C. Avendano, E.A. Mueller and G. Jackson, J. Chem. Phys. **148**, 164701 (2018).
[287] G.D. Wall and D.J. Cleaver, Phys. Rev. E **56**, 4306–4316 (1997).
[288] E. Caneda-Guzman, J.A. Moreno-Razo, E. Diaz-Herrera and E.J. Sambriski, Molec.

Phys. **112**, 1149–1159 (2014).
[289] C.C. Huang, M. Baus and J.P. Ryckaert, Molec. Phys. **113**, 2643–2655 (2015).
[290] D. Salgado-Blanco, C.I. Mendoza, M.A. Chavez-Rojo, J.A. Moreno-Razo and E. Diaz-Herrera, Soft Matter **14**, 2846–2859 (2018).
[291] D. Salgado-Blanco, E. Díaz-Herrera and C.I. Mendoza, J. Phys. Cond. Mat. **31**, 105101 (2019).
[292] D.A. Luzhbin and Y.L. Chen, Macromolecules **49**, 6139–6147 (2016).
[293] S.A. Egorov, A. Milchev, P. Virnau and K. Binder, J. Chem. Phys. **144**, 174902 (2016).
[294] S.A. Egorov, A. Milchev and K. Binder, Macrom. Theor. Simul. **26**, 1600036 (2017).
[295] A. Milchev, S.A. Egorov and K. Binder, Soft Matter **13**, 1888–1903 (2017).
[296] D.J. Cleaver and P.I.C. Teixeira, Chem. Phys. Lett. **338**, 1–6 (2001).
[297] P.I.C. Teixeira, F. Barmes, C. Anquetil-Deck and D.J. Cleaver, Phys. Rev. E **79**, 011709 (2009).
[298] C. Anquetil-Deck and D.J. Cleaver, Phys. Rev. E **82**, 031709 (2010).
[299] C. Anquetil-Deck, D.J. Cleaver and T.J. Atherton, Phys. Rev. E **86**, 041707 (2012).
[300] C. Anquetil-Deck, D.J. Cleaver, J.P. Bramble and T.J. Atherton, Phys. Rev. E **88**, 012501 (2013).
[301] A. DeBenedictis, T.J. Atherton, C. Anquetil-Deck, D.J. Cleaver, D.B. Emerson, M. Wolak and J.H. Adler, Phys. Rev. E **92**, 042501 (2015).
[302] M. Greschek, M. Melle and M. Schoen, Soft Matter **6**, 1898–1909 (2010).
[303] M. Greschek and M. Schoen, Soft Matter **6**, 4931–4941 (2010).
[304] M. Greschek and M. Schoen, J. Chem. Phys. **135**, 204702 (2011).
[305] M. Greschek, K.E. Gubbins and M. Schoen, J. Chem. Phys. **137**, 144703 (2012).
[306] D.L. Cheung, J. Chem. Phys. **128**, 194902 (2008).
[307] S. Okushima and T. Kawakatsu, Phys. Rev. E **96**, 052704 (2017).
[308] M. Ricci, M. Mazzeo, R. Berardi, P. Pasini and C. Zannoni, Faraday Disc. Chem. Soc. **144**, 171–185 (2010).
[309] T. Koda, M. Uchida, A. Nishioka, O. Haba, K. Yonetake, M. Kwak, Y. Momoi, N. Kim, S. Hong, D. Kang and Y. Choi, Mol. Cryst. Liq. Cryst. **612**, 24–32 (2015).
[310] T. Koda, Y. Hyodo, Y. Momoi, M. Kwak, D. Kang, Y. Choi, A. Nishioka, O. Haba and K. Yonetake, J. Phys. Soc. Japan **85**, 024601 (2016).
[311] W.L. Zhang, E.D. Gomez and S.T. Milner, Soft Matter **12**, 6141–6147 (2016).
[312] M.B. Hamaneh and P.L. Taylor, Phys. Rev. E **77**, 021707 (2008).
[313] M.F. Palermo, F. Bazzanini, L. Muccioli and C. Zannoni, Liq. Cryst. **44**, 1764–1774 (2017).
[314] A. Pizzirusso, R. Berardi, L. Muccioli, M. Ricci and C. Zannoni, Chem. Sci. **3**, 573–579 (2012).
[315] O.M. Roscioni, L. Muccioli, R.G. Della Valle, A. Pizzirusso, M. Ricci and C. Zannoni, Langmuir **29**, 8950–8958 (2013).
[316] H. Ramezani-Dakhel, M. Sadati, M. Rahimi, A. Ramirez-Hernandez, B. Roux and J.J. de Pablo, J. Chem. Theor. Comput. **13**, 237–244 (2017).
[317] H. Ramezani-Dakhel, M. Rahimi, J. Pendery, Y.K. Kim, S. Thayumanavan, B. Roux, N.L. Abbott and J.J. de Pablo, ACS Appl. Mater. Int. **10**, 37618–37624 (2018).
[318] O.M. Roscioni, L. Muccioli and C. Zannoni, ACS Appl. Mater. Int. **9**, 11993–12002 (2017).
[319] P. Popov, D.J. Lacks, A. Jakli and E.K. Mann, J. Chem. Phys. **141**, 054901 (2014).
[320] M. Li, H. Lai, B.X. Chen, X.Y. Liu and Y. Gu, Liq. Cryst. **37**, 149–158 (2010).
[321] O. Gürbulak and E. Cebe, J. Disp. Sci. Tech. **39**, 655–664 (2017).
[322] O. Gürbulak and E. Cebe, J. Molec. Liquids **256**, 611–619 (2018).
[323] O. Gürbulak and E. Cebe, Chinese Phys. Lett. **35**, 046802 (2018).
[324] T.J. Smith, W. Iglesias, S.R. Stefanovic, E.K. Mann, C. Tschierske, A. Jakli and D.J. Lacks, J. Phys. Chem. B **115**, 12809–12815 (2011).
[325] W. Iglesias, T.J. Smith, P.B. Basnet, S.R. Stefanovic, C. Tschierske, D.J. Lacks, A. Jakli and E.K. Mann, Soft Matter **7**, 9043–9050 (2011).

[326] W. Iglesias, T.J. Smith, P.B. Basnet, S. Stefanovic, C. Tschierske, D.J. Lacks, A. Jakli and E.K. Mann, Ferroelectrics **431**, 141–149 (2012).
[327] T.J. Smith, W. Iglesias, E.K. Mann, A. Jakli and D.J. Lacks, Liq. Cryst. **40**, 159–164 (2013).
[328] G. Watanabe, J.I. Saito, N. Kato and Y. Tabe, J. Chem. Phys. **134**, 054513 (2011).
[329] T.D. Nguyen, J.M.Y. Carrillo, M.A. Matheson and W.M. Brown, Nanoscale **6**, 3083–3096 (2014).
[330] D. Vanzo, M. Ricci, R. Berardi and C. Zannoni, Soft Matter **12**, 1610–1620 (2016).
[331] Q. Ji, R. Lefort and D. Morineau, Chem. Phys. Lett. **478**, 161–165 (2009).
[332] Q. Ji, R. Lefort, A. Ghoufi and D. Morineau, Chem. Phys. Lett. **482**, 234–238 (2009).
[333] Q. Ji, R. Lefort, R. Busselez and D. Morineau, J. Chem. Phys. **130**, 234501 (2009).
[334] S.I. Hernandez, J.A. Moreno-Razo, A. Ramirez-Hernandez, E. Diaz-Herrera, J.P. Hernandez-Ortiz and J.J. de Pablo, Soft Matter **8**, 1443–1450 (2012).
[335] J. Karjalainen, J. Lintuvuori, V.V. Telkki, P. Lantto and J. Vaara, Phys. Chem. Chem. Phys. **15**, 14047–14057 (2013).
[336] Y. Trukhina and T. Schilling, Phys. Rev. E **77**, 011701 (2008).
[337] P.X. Viveros-Mendez, A. Gil-Villegas and S.A. Espinoza, J. Chem. Phys. **147**, 234902 (2017).
[338] S.A. Egorov, A. Milchev and K. Binder, Phys. Rev. Lett. **116**, 187801 (2016).
[339] A. Milchev, S.A. Egorov, A. Nikoubashman and K. Binder, J. Chem. Phys. **146**, 194907 (2017).
[340] A. Nikoubashman, D.A. Vega, K. Binder and A. Milchev, Phys. Rev. Lett. **118**, 217803 (2017).
[341] A. Milchev, S.A. Egorov, D.A. Vega, K. Binder and A. Nikoubashman, Macromolecules **51**, 2002–2016 (2018).
[342] D. Caprion, Euro. Phys. J. E **28**, 305–313 (2009).
[343] R. Busselez, C.V. Cerclier, M. Ndao, A. Ghoufi, R. Lefort and D. Morineau, J. Chem. Phys. **141**, 134902 (2014).
[344] M. Tasinkevych and D. Andrienko, Cond. Matt. Phys. **13**, 33603 (2010).
[345] M. Ravnik and S. Žumer, Mol. Cryst. Liq. Cryst. **594**, 2–10 (2014).
[346] J.L. Billeter and R.A. Pelcovits, Phys. Rev. E **62**, 711–717 (2000).
[347] D. Andrienko, G. Germano and M.P. Allen, Phys. Rev. E **63**, 041701 (2001).
[348] J.A. Moreno-Razo, E.J. Sambriski, G.M. Koenig, E. Diaz-Herrera, N.L. Abbott and J.J. de Pablo, Soft Matter **7**, 6828–6835 (2011).
[349] J.M. Ilnytskyi, A. Trokhymchuk and M. Schoen, J. Chem. Phys. **141**, 114903 (2014).
[350] B.T. Gettelfinger, J.A. Moreno-Razo, G.M. Koenig, J.P. Hernandez-Ortiz, N.L. Abbott and J.J. de Pablo, Soft Matter **6**, 896–901 (2010).
[351] M.S. Al-Barwani, G.S. Sutcliffe and M.P. Allen, J. Phys. Chem. B **108**, 6663–6666 (2004).
[352] J.K. Whitmer, A.A. Joshi, T.F. Roberts and J.J. de Pablo, J. Chem. Phys. **138**, 194903 (2013).
[353] A. Humpert, S.F. Brown and M.P. Allen, Liq. Cryst. **45**, 59–69 (2018).
[354] S. Orlandi, E. Benini, I. Miglioli, D.R. Evans, V. Reshetnyak and C. Zannoni, Phys. Chem. Chem. Phys. **18**, 2428–2441 (2016).
[355] S. Orlandi and C. Zannoni, Mol. Cryst. Liq. Cryst. **573**, 1–9 (2013).
[356] S. Orlandi and C. Zannoni, Soft Matter **14**, 3882–3888 (2018).
[357] S. Bale, T.P. Liyana-Arachchi and F.R. Hung, Molec. Simul. **42**, 1242–1248 (2016).
[358] M. Rahimi, H. Ramezani-Dakhel, R. Zhang, A. Ramirez-Hernandez, N.L. Abbott and J.J. de Pablo, Nature Comm. **8**, 15064 (2017).
[359] M.P. Allen and D. Frenkel, Phys. Rev. A **37**, 1813–1816 (1988).
M.P. Allen and D. Frenkel, Phys. Rev. A **42**, 3641 (1990), Erratum.
[360] M.P. Allen, M.A. Warren, M.R. Wilson, A. Sauron and W. Smith, J. Chem. Phys. **105**, 2850–2858 (1996).
[361] A. Humpert and M.P. Allen, Molec. Phys. **113**, 2680–2692 (2015).
[362] P.A.C. O'Brien, M.P. Allen, D.L. Cheung, M. Dennison and A. Masters, Phys. Rev. E

78, 051705 (2008).
[363] P.A.C. O'Brien, M.P. Allen, D.L. Cheung, M. Dennison and A. Masters, Soft Matter **7**, 153–162 (2011).
[364] A.A. Joshi, J.K. Whitmer, O. Guzman, N.L. Abbott and J.J. de Pablo, Soft Matter **10**, 882–893 (2014).
[365] H. Sidky and J.K. Whitmer, Liq. Cryst. **43**, 2285–2299 (2016).
[366] H. Sidky, J.J. de Pablo and J.K. Whitmer, Phys. Rev. Lett. **120**, 107801 (2018).
[367] H. Steuer and S. Hess, Phys. Rev. Lett. **94**, 027802 (2005).
[368] J. Stelzer, R. Berardi and C. Zannoni, Chem. Phys. Lett. **299**, 9–16 (1999).
[369] J.L. Billeter and R.A. Pelcovits, Liq. Cryst. **27**, 1151–1160 (2000).
[370] A. Dewar and P.J. Camp, J. Chem. Phys. **123** (17), 174907 (2005).
[371] D.L. Cheung, S.J. Clark and M.R. Wilson, J. Chem. Phys. **121** (18), 9131–9139 (2004).
[372] T. Miyazaki and M. Yamashita, Ferroelectrics **365**, 115–121 (2008).
[373] M.I. Capar, A. Nar, A.V. Zakharov and A.A. Vakulenko, Physics Sol. Stat. **53**, 435–441 (2011).
[374] M.I. Capar, A. Nar, A. Ferrarini, E. Frezza, C. Greco, A.V. Zakharov and A.A. Vakulenko, J. Chem. Phys. **138**, 114902 (2013).
[375] J.S. van Duijneveldt and M.P. Allen, Molec. Phys. **90**, 243–250 (1997).
[376] M.A. Bates and G.R. Luckhurst, J. Chem. Phys. **120**, 394–403 (2004).
[377] R.L.B. Selinger, Phys. Rev. E **65**, 051702 (2002).
[378] G. Cinacchi and L. De Gaetani, Phys. Rev. E **79**, 011706 (2009).
[379] G. Cinacchi and L. De Gaetani, J. Chem. Phys. **131**, 104908 (2009).
[380] G. Cinacchi and L. De Gaetani, Phys. Rev. Lett. **103**, 257801 (2009).
[381] M. Piedrahita, A. Cuetos and B. Martinez-Haya, Soft Matter **11**, 3432–3440 (2015).
[382] A. Patti, D.E. Masri, R. van Roij and M. Dijkstra, Phys. Rev. Lett. **103**, 248304 (2009).
[383] A. Patti, D.E. Masri, R. van Roij and M. Dijkstra, J. Chem. Phys. **132**, 224907 (2010).
[384] A. Patti and A. Cuetos, Phys. Rev. E **86**, 011403 (2012).
[385] R. Matena, M. Dijkstra and A. Patti, Phys. Rev. E **81**, 021704 (2010).
[386] K.M. Aoki, Mol. Cryst. Liq. Cryst. **612**, 72–80 (2015).
[387] B. Mukherjee, C. Peter and K. Kremer, Phys. Rev. E **88**, 010502 (2013).
[388] B. Mukherjee, C. Peter and K. Kremer, J. Chem. Phys. **147**, 114501 (2017).
[389] M.G. Mazza, M. Greschek, R. Valiullin, J. Karger and M. Schoen, Phys. Rev. Lett. **105**, 227802 (2010).
[390] M.G. Mazza, M. Greschek, R. Valiullin and M. Schoen, Phys. Rev. E **83**, 051704 (2011).
[391] T. Stieger, M.G. Mazza and M. Schoen, Int. J. Mol. Sci. **13**, 7854–7871 (2012).
[392] T. Mima and K. Yasuoka, Phys. Rev. E **77**, 011705 (2008).
[393] S. Belli, A. Patti, R. van Roij and M. Dijkstra, J. Chem. Phys. **133**, 154514 (2010).
[394] A. Patti, S. Belli, R. van Roij and M. Dijkstra, Soft Matter **7**, 3533–3545 (2011).
[395] O. Cienega-Cacerez, J.A. Moreno-Razo, E. Diaz-Herrera and E.J. Sambriski, Soft Matter **10**, 3171–3182 (2014).
[396] S. Sarman and A. Laaksonen, Chem. Phys. Lett. **479**, 47–51 (2009).
[397] S. Sarman and A. Laaksonen, J. Chem. Phys. **131**, 144904 (2009).
[398] S. Sarman, Y.L. Wang and A. Laaksonen, Phys. Chem. Chem. Phys. **17**, 16615–16623 (2015).
[399] S. Sarman, Y.L. Wang and A. Laaksonen, J. Chem. Phys. **144**, 054901 (2016).
[400] S. Sarman and A. Laaksonen, Phys. Chem. Chem. Phys. **17**, 3332–3342 (2015).
[401] S. Sarman and A. Laaksonen, Phys. Chem. Chem. Phys. **14**, 11999–12013 (2012).
[402] G.R. Luckhurst and K. Satoh, J. Chem. Phys. **132**, 184903 (2010).
[403] S. Sarman and D.J. Evans, J. Chem. Phys. **99**, 9021–9036 (1993).
[404] D.L. Cheung, S.J. Clark and M.R. Wilson, Chem. Phys. Lett. **356**, 140–146 (2002).
[405] J. Kim, M. Jamil, J.E. Jung, J.E. Jang, A. Farzana, W.L. Jin, W.P. Sang, M.K. Woo, J.Y. Kwak and Y.J. Jeon, Chinese J. Chem. **29**, 48–52 (2011).
[406] Q. Wang, G. Zhang, Y. Liu, L. Yao, D. Li, S. Wang, Z. Cao, Q. Mu, C. Yang, L. Xuan, X. Lu and Z. Peng, Liq. Cryst. **45**, 129–135 (2018).

[407] Z. Ran, P. Zeng-Hui, L. Yong-Gang, Z. Zhi-Gang and X. Li, Chinese Phys. B **18**, 4380–4385 (2009).
[408] M.I. Capar, E. Cebe and A.V. Zakharov, Chem. Phys. Lett. **514**, 124–127 (2011).
M.I. Capar, E. Cebe and A.V. Zakharov, Chem. Phys. Lett. **524**, 116 (2012), Erratum.
[409] A. Humpert and M.P. Allen, Phys. Rev. Lett. **114**, 028301 (2015).
[410] A. Humpert, A.J. Masters and M.P. Allen, Euro. Phys. J. Spec. Top. **225**, 1723–1732 (2016).
[411] M. Ripoll, R.G. Winkler, K. Mussawisade and G. Gompper, J. Phys. Cond. Mat. **20**, 404209 (2008).
[412] M. Ripoll, Phys. Rev. E **83**, 040701 (2011).
[413] R.G. Winkler, S.P. Singh, C.C. Huang, D.A. Fedosov, K. Mussawisade, A. Chatterji, M. Ripoll and G. Gompper, Euro. Phys. J. Spec. Top. **222**, 2773–2786 (2013).
[414] W. Chen, S. Kulju, A.S. Foster, M.J. Alava and L. Laurson, Phys. Rev. E **90**, 012404 (2014).
[415] C. Manzato, A.S. Foster, M.J. Alava and L. Laurson, Phys. Rev. E **91** (2015).
[416] Y.W. Zhang, X.S. Chen and W. Chen, Commun. Theor. Phys. **66**, 467–473 (2016).
[417] A. Sunarso, T. Tsuji and S. Chono, Appl. Phys. Lett. **93**, 244106 (2008).
[418] A. Sunarso, T. Tsuji and S. Chono, J. Appl. Phys. **110**, 044911 (2011).
[419] R. Berardi, L. Muccioli and C. Zannoni, J. Chem. Phys. **128**, 024905 (2008).
[420] M. Ricci, R. Berardi and C. Zannoni, J. Chem. Phys. **143**, 084705 (2015).
[421] K. Goossens, K. Lava, C.W. Bielawski and K. Binnemans, Chem. Rev. **116**, 4643–4807 (2016).
[422] C. Avendano, A. Gil-Villegas and E. Gonzalez-Tovar, J. Chem. Phys. **128**, 044506 (2008).
[423] G. Jimenez-Serratos, C. Avendano, A. Gil-Villegas and E. Gonzalez-Tovar, Molec. Phys. **109**, 27–36 (2011).
[424] C. Avendano, A. Gil-Villegas and E. Gonzalez-Tovar, Chem. Phys. Lett. **470**, 67–71 (2009).
[425] T. Margola, G. Saielli and K. Satoh, Mol. Cryst. Liq. Cryst. **649**, 50–58 (2017).
[426] T. Margola, K. Satoh and G. Saielli, Crystals **8**, 371 (2018).
[427] G. Saielli, T. Margola and K. Satoh, Soft Matter **13**, 5204–5213 (2017).
[428] H. Bartsch, M. Bier and S. Dietrich, J. Phys. Cond. Mat. **29**, 464002 (2017).
[429] G.C. Ganzenmüller and G.N. Patey, Phys. Rev. Lett. **105**, 137801 (2010).
[430] E. Trizac, L. Bocquet, R. Agra, J.J. Weis and M. Aubouy, J. Phys. Cond. Mat. **14**, 9339–9352 (2002).
[431] R. Agra, E. Trizac and L. Bocquet, Euro. Phys. J. E **15**, 345–357 (2004).
[432] L. Morales-Anda, H.H. Wensink, A. Galindo and A. Gil-Villegas, J. Chem. Phys. **136**, 034901 (2012).
[433] S. Jabbari-Farouji, J.J. Weis, P. Davidson, P. Levitz and E. Trizac, Scientific Reports **3**, 3559 (2013).
[434] S. Jabbari-Farouji, J.J. Weis, P. Davidson, P. Levitz and E. Trizac, J. Chem. Phys. **141**, 224510 (2014).
[435] M. Delhorme, C. Labbez and B. Jonsson, J. Phys. Chem. Lett. **3**, 1315–1320 (2012).
[436] M. Delhorme, B. Jonsson and C. Labbez, Soft Matter **8**, 9691–9704 (2012).
[437] M. Delhorme, B. Jonsson and C. Labbez, RSC Advances **4**, 34793–34800 (2014).
[438] Y. Wang, S. Feng and G.A. Voth, J. Chem. Theor. Comput. **5**, 1091–1098 (2009).
[439] Y. Wang, W.G. Noid, P. Liu and G.A. Voth, Phys. Chem. Chem. Phys. **11**, 2002–2015 (2009).
[440] G. Saielli, Soft Matter **8**, 10279–10287 (2012).
[441] G. Saielli, G.A. Voth and Y.T. Wang, Soft Matter **9**, 5716–5725 (2013).
[442] G. Saielli, A. Bagno and Y.T. Wang, J. Phys. Chem. B **119**, 3829–3836 (2015).
[443] Y.M. Ji, R. Shi, Y.T. Wang and G. Saielli, J. Phys. Chem. B **117**, 1104–1109 (2013).
[444] G. Saielli and Y.T. Wang, J. Phys. Chem. B **120**, 9152–9160 (2016).
[445] D. Frezzato and G. Saielli, J. Phys. Chem. B **120**, 2578–2585 (2016).
[446] G. Saielli, J. Phys. Chem. B **120**, 2569–2577 (2016).

[447] M.J. Quevillon and J.K. Whitmer, Materials **11**, 64 (2018).
[448] M.R. Schenkel, J.B. Hooper, M.J. Moran, L.A. Robertson, D. Bedrov and D.L. Gin, Liq. Cryst. **41**, 1668–1685 (2014).
[449] D. Andrienko, J. Kirkpatrick, V. Marcon, J. Nelson and K. Kremer, Physica Stat. Sol. B **245**, 830–834 (2008).
[450] J. Kirkpatrick, V. Marcon, K. Kremer, J. Nelson and D. Andrienko, J. Chem. Phys. **129**, 094506 (2008).
[451] V. Marcon, T. Vehoff, J. Kirkpatrick, C. Jeong, D.Y. Yoon, K. Kremer and D. Andrienko, J. Chem. Phys. **129**, 094505 (2008).
[452] S. Bag, V. Maingi, P.K. Maiti, J. Yelk, M.A. Glaser, D.M. Walba and N.A. Clark, J. Chem. Phys. **143**, 144505 (2015).
[453] G. Cinacchi, R. Colle, P. Parruccini and A. Tani, J. Chem. Phys. **129**, 174708 (2008).
[454] L.A. Haverkate, M. Zbiri, M.R. Johnson, B. Deme, F.M. Mulder and G.J. Kearey, J. Phys. Chem. B **115**, 13809–13816 (2011).
[455] M. Goto, H. Takezoe and K. Ishikawa, J. Chem. Phys. **132**, 054506 (2010).
[456] T.A. Papadopoulos, L. Muccioli, S. Athanasopoulos, A.B. Walker, C. Zannoni and D. Beljonne, Chem. Sci. **2**, 1025–1032 (2011).